Discussion and Redevelopment

In principle, Fixman's theory contains no adjustable parameters. The two central microscopic parameters κ and h may be derived from some light-scattering data[15]; also, thermodynamic data could be used for κ through its relation to $(\partial\mu_1/\partial n_2)$ in Eq. (26). Practically, the theory has always been used with h and κ as two adjustable parameters to be set from a least-squares fit of the absorption α or α/f^2 as a function of frequency f and temperature T at the critical composition. (Extension of the theory for the composition dependence of α has also been done.) To reduce κ, which varies with temperature, to a fixed parameter, the Debye[11] relation is used,

$$\kappa^2 = \frac{6}{\ell^2}\,\frac{|T-T_c|}{T_c} \quad , \tag{39}$$

ℓ being the Debye persistence length. This last step fixes the theory squarely in classical critical thermodynamics, as the compressibility then diverges as $\underline{|T-T_c|^{-1}}$. Similarly, a Flory-Huggins type[11,16] model for the chemical potential μ_1,

$$\mu_1 = kT\left[\ell n\ \phi_1 + a\phi_2 + b\phi_2^{\,2}\right] \tag{40}$$

is used to set the constant a of Eq. (26), since the diffusion constant h can be expressed through an involved reduction[13] in terms of equivalent ideal diffusion constants in the form

$$h = H/a\zeta \ , \qquad (41)$$

where ζ is a molecular friction constant of more intuitive value.

Overall then, Fixman theory as used in analyzing experimental data incorporates several classical thermodynamic models—the two above, plus the Ornstein-Zernike model for $G(R)$ which can be made partially non-classical by letting κ^2 have its true order of zero at T_c. None of this compromises the theory, which is necessarily classical from the point where an integer order (second) expansion of δG in terms of δn_2 is taken. The restriction is more apparent in the final expression for α, proportional to $(\partial\kappa^2/\partial T)$ - the classical relation Eq. (39) gives an α neither divergent nor vanishing at T_c, while the true critical behavior of κ^2 has a higher than linear relation to $|T-T_c|$ and would yield $\alpha=0$ at the critical point. At modest distances from the critical point at the mere onset of the anomaly, the deviation from classicality should be tolerable and the theory valid. In its usage to date on data quite near critical, Fixman theory yields more questionable parameters. We return to this point after discussing the relative success of the theory as well as competing theories.

In application to various sets of experimental data on binary consolute points, Fixman's theory has been qualitatively upheld in most respects. The early data of Chynoweth and Schneider[17] on aniline/n-hexane at one frequency was analyzed by Fixman in his original paper, finding the predicted temperature dependence. The temperature derivative of the velocity, $d\beta/dT$, was positive and half as large as predicted. Anantaraman, et al.[18] found good f- and T-dependence, but $d\beta/dT < 0$ contrary to expectations in nitrobenzene/isooctane. D'Arrigo and Sette[19] found adequate T-dependence and again $d\beta/dT < 0$ in nitrobenzene/n-hexane. They also give a form for the composition or X-dependence of α/f^2 based on keeping the $\bar{V}_2/\bar{V}_1$ term in Eq. (26). This yields a peak in α/f^2 in composition that was far too narrow, due to the need to use the Flory-Huggins model for $(\partial\mu_1/\partial n_2)$ with its inherent limitation to a quadratic coexistence curve rather than the flatter, cubic true curve. Limited work on nitroethane/isooctane by Shakhparonov, et al.[20] showed an f-dependence fitting a power law like $\alpha/f^2 \sim f^{-(p+1)}$, with p in the range (0,1), roughly consistent with the $f^{-5/4}$ dependence predicted for small $|T-T_c|$. Puls[22] studied the liquid metal system Ga/Bi as one of the simplest binaries, finding fair f- and T-dependence and $d\beta/dT \approx 0$. The X-dependence was fair but still too narrow. Interestingly, α/f^2 predicted with the persistence length ℓ set from the least-squares fit and ζ calculated from an estimate of the ideal diffusion constant, was 6.5 times too large, again reflecting the defects of classical thermodynamics, this time for the fluctuation spectrum $\delta n_2^{\,2}$.

Attempts have been made to avoid the defects of Fixman theory regarding mathematical rigor or thermodynamics in the rival theories of Kawasaki[23] and of Kadanoff and Swift.[24] Kawasaki[23a] originally gave a treatment based on the autocorrelation function expression for the combination of (frequency-dependent) shear and bulk viscosities,

$$\Theta = \frac{4}{3}\,\eta_S + \eta_B \; . \tag{42}$$

The anomalous absorption from the shear viscosity anomaly is automatically included, unlike Fixman's treatment. The fluxes in the autocorrelation function are expanded to second order in the concentration fluctuations, and for the equation of motion of the latter Fixman's form Eq. (25) is used, as also the Ornstein-Zernike form for the equilibrium average fluctuations. Kawasaki's result is substantially that of Fixman but for the change from isobaric to adiabatic propagation conditions, which is minor. It is similarly restricted to classical thermodynamics, again due to the quadratic expansion of quantities (here, the fluxes) of thermodynamic significance. The theory of Kadanoff and Swift[24] incorporates a perturbation solution of the master equation, using the so-called dynamic scaling laws. Though the derivation is quite involved, their result for the critical region behavior of the quantity θ, hence of α, is that it diverges as $\underline{|T-T_c|^{-2+A}}$—where $\underline{A}$ is the critical exponent of the heat capacity C_p—and is independent of frequency. Kawasaki's[23b] extended theory is also a dynamic scaling theory that extends to the non-hydrodynamic region of sound frequency where the condition (31) is reversed. He also incorporates a quadratic expansion for the fluxes, which is classical thermodynamics. His results are the frequency and temperature exponents for absorption divergence, similar to Kadanoff and Swift.

As Kawasaki's original theory is essentially a corroboration of Fixman's, and as the form

$$\frac{\alpha}{f^2} \sim |T-T_c|^{-p} \text{ (times } f^{-q}\text{, possibly)} \tag{43}$$

predicted by Kadanoff and Swift or by Kawasaki in his extended theory is not observed and in addition the dynamic scaling laws are unproven,[25] we may take Fixman theory as the one of primary utility in analyzing experimental results. Its defects are only partly remediable. One that can be fixed is the expression of the dynamic response of $(\delta \underline{n_2})^2 = \underline{n_2^2 \int d\vec{k}}\, G_{\vec{k}}$ to the perturbation $\delta \underline{T}$. Here $\delta \underline{G_{\vec{k}}}$ can be computed *after* solution of the proper singlet diffusion equation. Assuming the Fourier decomposition (23a) for the *undriven* fluctuation plus a decomposition for the driven portion $\delta \underline{n_2}^d$,

$$\delta n_2{}^d = \int n_{\vec{k}}^d \, e^{i\vec{k}\cdot\vec{R}} \, d\vec{k} \ , \tag{44}$$

the perturbation solution is

$$[i\omega + \frac{h}{2} k^2 \ (k^2 + \kappa^2)] \ n_k^d = \frac{h}{2} k^2 \frac{\partial \kappa^2}{\partial T} \delta T \ n_{\vec{k}}^o \ .$$

Then

$$n_2^2 \ \delta G_{\vec{k}} = \langle n_k^o \ n_{\vec{k}}^d \rangle + \langle n_{\vec{k}}^d \ n_{\vec{k}}^o \rangle = 2 \ \langle n_{\vec{k}}^o \ n_{\vec{k}}^d \rangle \tag{45}$$

and

$$\int dk \ G_{\vec{k}} = \delta T \ h \left(\frac{\partial \kappa^2}{\partial T}\right) \int d\vec{k} \ \frac{k^2 G_{\vec{k}}^o}{[i\omega + \frac{h}{2} k^2 \ (k^2 + \kappa^2)]}, \tag{46}$$

and δS has the form of Eq. (33) but for the replacement of h in the denominator of the integral over k by $h/2$. According to this correction, values of the parameters ℓ and ζ derived from the original theory should be multiplied by $2^{-7/3} = 0.20$ and $2^{1/3} = 1.26$, respectively. As the parameters ℓ, a, ζ backed out of the data by Fixman theory are generally order-of-magnitude, this is not a dramatic change, and certainly not a change of philosophy.

Another point of rigor that can be resolved is Fixman's choice of the term in Eq. (30) as the dominant perturbation. We know that the new driving term must be linear in the ultrasonic progress variables δp, δT, and also that the separate linear terms in $\nabla^2 T$ and $\nabla^2 p$ cause no anomaly. Therefore, we require a perturbation to the coefficients of c_2 in the diffusion equation. Here the main sensitivity to δT or δP is in κ^2. In a recent thesis, Puls[26] notes that a term in δp analogous to term (30) is neglected by Fixman yet may be significant. Now the δT term originated in the derivative

$$\left(\frac{\partial \kappa^2}{\partial T}\right) \delta T \sim \frac{\partial^2 \mu_1}{\partial T \partial c_2} \delta T = \frac{\partial^3 G_{mix}}{\partial N_1 \partial T \partial c_2} \delta T, \qquad (47)$$

where G_{mix} is the Gibbs energy of mixing of an arbitrary mass and the derivative with respect to N_1 is at constant

$N_{\cancel{1}\lambda}$. The analogous pressure term is

$$\frac{\partial^2}{\partial N_1 \partial c_2} \left(\frac{\partial G_{mix}}{\partial p}\right) \delta p = \frac{\partial^2}{\partial N_1 \partial c_2} \Delta V_{mix} \ \delta p, \tag{48}$$

where V_{mix} is the volume change on mixing. The ratio of (48) to (47) is

$$\frac{\left(\frac{\partial^2 \Delta V_{mix}}{\partial N_1 \partial c_2}\right)}{\left(\frac{\partial^2 \mu_1}{\partial T \partial c_2}\right)} \frac{\delta p}{\delta T} = \frac{\left(\frac{\partial^2 \Delta V_{mix}}{\partial N_1 \partial c_2}\right)}{\left(\frac{\partial^2 \mu_1}{\partial T \partial c_2}\right)} \frac{C_p}{TV\theta} . \tag{49}$$

Using the Flory-Huggins model for $(\partial^2\mu_1/\partial c_2\partial T)$ and experimental density data for $(\partial^2\Delta V_{mix}/\partial N_1\partial c_2)$, we have evaluated this ratio for the system 2,6-lutidine/water reported in the following paper[27] and have found it to be roughly -7.9%. In general the δp term should be negligible.

In light of the previous discussion, the defects of the theory as valid classical thermodynamics and hydrodynamics are resolved. The inherent deficiency of classical thermodynamics is difficult to remedy and we can see no path for improvement at present, with or without incorporating features of the other mode-coupling theories commented upon. One final point actually extrinsic to the theory is whether or not ordinary thermal relaxation involving driving of the same concentration variable $\underline{c_2}$ is truly additive to the Fixman mechanism. Intuitively, it appears so, as the two mechanisms involve vastly different spatial scales or $\underline{n_{\vec{k}}}$ components: the former involves structure on the order of one or two molecular diameters, the latter, structure on the order of hundreds of Angstroms. On a more rigorous basis, the two mechanisms are seen to drive distinct linear terms in the $\delta\underline{S}$ and $\delta\underline{V}$ expressions, Fixman's driving an added heat capacity in the first term in Eq. (5) and (6). As Eqs. (5) and (6) are combined to calculate the effective complex compressibility, the terms of the two types occur linearly and thus additively. This additivity of thermal relaxation is commonly employed in analyzing experimental data, and it is found particularly important for the lutidine/water system we have studied.

References

1. A. B. Bhatia, *Ultrasonic Absorption* (Clarendon Press: Oxford, 1967); K. F. Herzfeld and T. A. Litovitz, *Absorption and Dispersion of Ultrasonic Waves* (Academic Press: New York, 1959); W. P. Mason, ed., *Physical Acoustics* (Academic Press: New York, continuing series); S. Flügge, ed., *Handbuch der Physik*, Vol. XI/1 (Springer-Verlag: Berlin, 1961).

2. Early indications are in references 1-8 of M. Fixman, J. Chem. Phys. **33**, 1363 (1960).

3. R. Lucas, J. Phys. Rad. **8**, 41 (1937).

4. A. E. Brown and E. G. Richardson, Phil. Mag. **4**, 705 (1959); A. E. Brown, Acustica **18**, 169 (1967).

5. M. Fixman, J. Chem. Phys. **36**, 1961 (1962).

6. We follow the notation and development of Bhatia (ref. 1), pp. 174 ff.

7. R. M. Mazo, J. Chem. Phys. **28**, 1223 (1958).

8. L. D. Landau and E. M. Lifshitz, *Fluid Mechanics* (Addison-Wesley Publ. Co.: Reading, Mass., 1959), Chapter VI.

9. M. Fixman, J. Chem. Phys. **36**, 1957 (1962).

10. L. S. Ornstein and F. Zernike, physik. Z. **19**, 134 (1918); a more recent discussion is given by M. E. Fisher, J. Math. Phys. **5**, 944 (1964).

11. M. Fixman, J. Chem. Phys. **36**, 310 (1962); actual derivation by P. Debye, *ibid.* **31**, 680 (1959), and by M. Fixman, *ibid.* **33**, 1357, (1960).

12. M. Fixman, J. Chem. Phys. **36**, 310 (1962), Section A.

13. *Ibid.*, Eqs. (22), (23), and Section VIII.

14. ref. 5, Eq. (6).

15. R. D. Mountain, J. Chem. Phys. **38**, 205 (1966); with J. M. Deutch, *ibid*, **50**, 1103 (1969).

16. J. H. Hildebrand and R. L. Scott, *Solubility of Nonelectrolytes* (Reinhold Publ. Corp.: New York, 1950).

17. A. G. Chynoweth and W. G. Schneider, J. Chem. Phys. *19*, 1566 (1951); *20*, 760 (1952).

18. A. V. Anantaraman, A. B. Walters, P. D. Edmonds, and C. J. Pings, J. Chem. Phys. *44*, 2651 (1966).

19. G. D'Arrigo and D. Sette, J. Chem. Phys. *48*, 691 (1968).

20. M. I. Shakhparonov, Yu. G. Shoroshev, S. S. Aliev, P. K. Khabibullaev, and L. V. Lanshina, Sov. Phys. - JETP Letters *7*, 315 (1968).

21. R. P. Singh and G. S. Verma, Proc. Phys. Soc. *1*, 1476 (1968).

22. M. P. Puls, thesis, McMaster Univ., May, 1970.

23. K. Kawasaki: a) Proc. Phys. Soc. *90*, 791 (1967); Phys. Rev. *150*, 291 (1966); b) *ibid.*, *A1*, 1750 (1970).

24. L. P. Kadanoff and J. Swift, Phys. Rev. *165*, 310 (1968); *166*, 89 (1968); J. Swift, *ibid*. *173*, 257 (1968).

25. L. P. Kadanoff, J. Phys. Soc. Japan Suppl. *26*, 122 (1969).

26. Puls, *op. cit.*, p. 136.

27. V. Gutschick and C. J. Pings, J. Chem. Phys. *xx*, xxxx (1971); following paper.

Ultrasonic Investigation of the Lower Consolute Point of the 2,6-Lutidine: Water System*

Vincent P. Gutschick† and C. J. Pings

Division of Chemistry and Chemical Engineering
California Institute of Technology,
Pasadena, California 91109

Sound absorption coefficients and velocities have been measured over ranges in frequency, temperature, and composition for 2,6-lutidine/water near its critical mixing point. Large excess absorption coupled to critical fluctuation dynamics is found, as in other binary mixtures. A strong background of ordinary thermal relaxation is also apparent. Interpretation of the details of the absorption and velocity, as well as of auxiliary data on the shear viscosity and density, in terms of the Fixman mechanism of critical region absorption combined with a chemical association model cannot be attempted quantitatively. The reason lies in defects in Fixman theory for the composition dependence of the critical absorption, and

---

* Research sponsored by AFOSR (SRC)-OAR, USAF Grant No. AFOSR-68-1382.

† National Science Foundation Predoctoral Fellow, 1966-1970.

in the inherent inability of the chemical association model to account for phase separation behavior. Nevertheless, Fixman's form for the absorption as a function of frequency and temperature at the critical composition is satisfactory, and some important qualitative aspects of binary fluid structure come to light, including inherent differences of upper and lower consolute points.

Introduction

Binary liquid mixtures commonly exhibit nonadditive thermodynamic and kinetic behavior, many of the details of which are manifested in the ultrasonic absorption coefficient α and velocity β. In some cases, chemical association of small numbers of the two basic species in a linked set of chemical reactions causes enthalpy, volume, and excess entropy changes on mixing. Values of these three parameters for each reaction, as well as relaxation times related to the forward or backward rate constants, can sometimes be extracted for the principal reactions by analyzing the ultrasonic data as a function of mixture composition and temperature and of sound frequency.[1] The periodic temperature and pressure perturbation alters the microscopic dynamics in a well-defined manner and causes a sound energy loss or absorption. Additionally, the chemical and physical associations may generate a free energy of mixing of such form as to cause a region of imperfect miscibility and a corresponding critical mixing (consolute) point of incipient phase separation. Large thermodynamic composition fluctuations or changes in large-scale association occur here, and these are also susceptible to the sonic perturbation. Added absorption and velocity dispersion arise, describable readily by a theory of Fixman[2] in terms of the Ornstein-Zernike correlation length κ or the Debye persistence length $\underline{\ell}$, plus a friction constant ζ.

Numerous investigations have been made on both the chemical relaxation loss mechanism, which we denote as thermal relaxation (TR) and the latter mechanism, which we call critical relaxation (CR). In most studies the system, composition, and temperature have been chosen to make one or the other mechanism dominant, especially in the absorption behavior. Our present work on the 2,6-lutidine/water system focuses on the critical losses, although a comparably large background of TR accompanies the CR. Our system was chosen because it has a lower consolute point, or phase separation above a critical temperature, rather than the typical upper consolute point. The critical point is conveniently close to room temperature. For the description of the CR portion of the absorption, we use Fixman's theory as presented in the preceding paper[3] (I), as it was shown there that CR and TR may be considered additive and that Fixman's CR theory has been reasonably successful in the past. A chemical association model for TR and equilibrium properties is also attempted. The original goal of our study was the quantitative understanding of the ultrasonic and equilibrium properties using these two models. While this has failed, we can pinpoint the precise difficulties in such an approach and also draw some significant qualitative conclusions on binary mixture structure, differences of upper and lower consolute points, and the adequacy of Fixman theory.

Experimental

The absorption α and the velocity β were measured at fourteen compositions over the whole range, at four frequencies, nominally 4.5, 7.5, 10.5, and 13.5 MHz, and at least two temperatures of $\underline{T_c}$ - 0.92 C and $\underline{T_c}$ - 0.12 C, plus a third temperature for most compositions as close to the phase separation temperature as practical but not exceeding $\underline{T_c}$ + 1.08 C. Supplementary data on the shear viscosity and density were also taken. The phase diagram of Cox and Herington[4] was used to help locate the critical composition and temperature.

The basic ultrasonic apparatus is a pulsed variable-path single pass cell, a modification of the typical design of Andreae, et al.[5a] Equipment used in previous investigations in our laboratory[5b] has been adapted, but with better temperature control and electronic stability.

The temperature is controlled with a circulating water jacket supplied from an external bath, and also a heated Lucite enclosure for the total apparatus. The sample is mixed, and its composition identified by density measured in a thermostatted pycnometer. It is introduced into the sample cell, which is immediately reassembled. An upper silica and a lower Duralumin delay rod carry the ultrasonic pulse to the liquid gap. After equilibration, measurements of the absorption coefficient α and the velocity β are made at all frequencies, the temperature is changed and the measurements repeated. In all ultrasonic measurement, pulses of 8 μsec. duration and one kHz repetition rate from a Chesapeake U-100 signal generator drive an X-cut transducer at low power. For path length variations, a Gaertner micrometer carries the upper delay rod through a Teflon seal. Horizontal and vertical alignment between the two rods is insured by several independent techniques. Both rods were initially finished to 0.1 mil or better, though the lower rod's surface deteriorated without noticeable bad effects. Absolute liquid path lengths are occasionally checked, for use in establishing diffraction corrections. Signal frequency is measured by visual beating against the calibrated reference signal generator. The received signal is preamplified in an

Arenberg PA-620L and displayed on a Tektronix 547 CRO, along with the reference signal from the Hewlett-Packard HP-606A. The reference signal is attenuated in calibrated steps of one db nominally by a Hewlett-Packard HP-355C attenuator and the liquid path changed to keep the two signal displays superposed. A least-squares fit of path length versus attenuation directly yields the absorption coefficient. Signal quality is good except that some mode conversion in the delay rods causes spurious signal envelope fluctuations, for which an empirical correction to the raw absorption coefficients is applied at the two lowest frequencies. Velocity measurements are made by varying the path length and restoring signal superposition with the calibrated variable delay of the CRO.

Raw path-length/decibel data were corrected for diffraction by calculations on the method of Bass.[6] They were then reduced to an attenuation coefficient by a least-squares fit, weighted by estimated visual matching and amplitude stability errors, and augmented by a students' t-test. A similar reduction averaged the repeated runs made, generally three to five. Finally, error estimates were rescaled to give a unity chi-squared. Accuracies of α values are typically 0.5% near peak α, on up to 5% for the lowest absorptions at $\underline{f}$ = 4.5 MHz.

Velocity accuracy is of the order of 0.3%. A total calibration run on reagent benzene titrating as 0.02% water produced the result $\alpha/\underline{f}^2 = 962\mathrm{x}10^{-17}$ Np. cm.$^{-1}$ sec.^{2} (Np. = neper = 8.686 db.), near the literature value[7] of 960 ± 15 in these units.

99% lutidine was used after refluxing over BaO and distilling; water content was typically 0.1 mole percent by titration. Laboratory distilled water was used. Initial density ↔ mole fraction identifications were established by making solutions by weight on an analytical balance. Temperatures of pycnometers in the thermostat and of samples in the cell were ordinarily read to ± 0.01 C. with glass thermometers calibrated against a Leeds and Northrup platinum resistance thermometer certified by the NBS. The latter was also used to establish the critical temperature and composition by visual observations of phase separation as $\underline{T_c} = 33.57$ C. and mole fraction $\underline{X_c} = 0.065 \pm 0.001$ lutidine, respectively, versus $\underline{T_c} = 34.06$ C. and $\underline{X_c} = 0.0665$ of reference 4. Sample composition in the ultrasonic cell was stabilized by an evaporation buffer in the line to the atmosphere, and cell corrosion was prevented by silver plating. Mixtures were ring-stirred in the cell (not during actual measurements). All temperatures were controlled to within the 0.03 C.

stability of the external bath. Independent thermocouple measurements indicated a drop of 0.01 C. between the external bath and the sample.

Auxiliary determinations of shear viscosity were made on separate samples with a Cannon-Fenske viscometer calibrated with distilled water and with reagent acetone. Corrections were made to the raw kinematic viscosities according to NBS monograph No. 55 to yield final accuracies of 1%.

Results

The corrected absorption coefficients are presented[8] in Figs. 1-3. They are presented in the form α/f^2, f being the sound frequency. Furthermore, the so-called classical[9] contribution α_{cl}/f^2 from ordinary viscous losses,

$$\frac{\alpha_{cl}}{f^2} = \frac{8\pi^2\eta_s}{3\ \rho\beta^3} \tag{1}$$

with η_s the shear viscosity, have been subtracted to leave the excess quantity α_{ex}/f^2 which is to be interpreted in terms of relaxation (or, formally, in terms of a bulk viscosity $\eta_v = \rho\beta^3\alpha_{ex}/2\pi^2 f^2$). Thermal conduction also causes a classical loss but is negligible in binary liquids. Typically α_{cl}/f^2 is of the order of 5% of α_{ex}/f^2, showing relaxation as the dominant loss mechanism. Fig. 1 presents α_{ex}/f^2 as a function of composition X = mole fraction lutidine for the temperature $T = T_c - 0.92$ C., with one curve for each of the four frequencies used. Figs. 2, 3 present similar results for temperatures T_c - 0.12 C., T_c + 1.08 C. Much structure in X- and f-dependence is evident; the T-dependence of α_{ex}/f^2 is also strong but less obvious.

The magnitude and frequency-dependence of α_{ex}/f^2 allows us to dismiss two loss mechanisms and to retain the CR-plus-TR explanation we have mentioned earlier. The first loss mechanism is scattering of sound[10] by the inhomogeneous acoustical impedance $\rho\beta$, ρ = density, in the presence of fluctuation. The frequency-dependence associated with such a mechanism is

$$\frac{\alpha_{ex}}{f^2} \sim f^p \quad , \quad 0 < p < 2 \, , \tag{2}$$

certainly not seen here although strong critical opalescence was seen in several of the states investigated. The small variation of $\rho\beta$ with macroscopic composition adds support to the conclusion. The second mechanism is the persistence of the excess absorption of the pure liquids, possibly as

$$\frac{\alpha_{ex}}{f^2} = X\left(\frac{\alpha_{ex}}{f^2}\right)_{\text{lutidine}} + (1-X)\left(\frac{\alpha_{ex}}{f^2}\right)_{\text{water}} \qquad (3)$$

$$\approx [70\,X + 18(1-X)] \times 10^{-17}\ \text{Np. cm. sec.}^{-2}$$

Our measured absorptions are considerably larger than this, and in addition, the contributions are less than additive due to cross-relaxation.[11]

Presumably all our data can be well represented as the sum of the CR and TR contributions,

$$\frac{\alpha_{ex}}{f^2} = Af^{-5/4}\,\mathcal{I}(d) + B\ , \qquad (4)$$

where

$$d = Cf^{-1/2}\,\kappa^2\ \left(=C'f^{-1/2}\,|T-T_c|\ \text{at}\ X=X_c\right) \qquad (5)$$

(see Ref. 18). The second term is actually composite,[12]

$$B \approx \sum_i \frac{Bi}{1 + (f/f_{ci})^2}$$

but all of the chemical relaxation times f_{ci} are almost surely higher than any frequencies we have used. B is primarily a strong function of composition X; it is also expected to have a modest and probably negative linear temperature dependence. It should peak at the composition of strongest chemical association. The first or CR term is translated from Fixman[2] form, with A, C known functions of X with weak dependence on T, and with $\mathcal{I}(d)$ a dimensionless monotonically decreasing function of d related to an excess dynamic heat capacity presented to the sound wave. The parameters A and C can be simply reduced to the parameters ζ and ℓ^2 or κ^2 of Fixman theory.

The TR absorption is quite extensive in composition, while its peak is strongly skewed, peaking near $X = 0.1$. It shows little f-dependence. The CR absorption peaks strongly at $X = X_c$ with strong f- and T-dependence. It is also quite extensive in X, as α/f^2 has significant f-dependence far from X_c, and its strong T-dependence extends to the TR peak, the base of which *lifts* with temperature as a result. Quantitative analysis of the results will be attempted below. Additional insight into the internal structure and dynamics is also provided by examining the sound velocity β at $f = 4.5$ MHz (its dispersion or f-dependence is low) and the sign of its temperature derivative, in Fig. 4; also the volume change on mixing, V_{mix}, in the same figure; the shear viscosity η_s as a function of composition at a typical temperature

$\underline{T_c}$ - 0.4 C. in Fig. 5; and the logarithmic temperature derivative $d\ell n\ \eta_s/dT$ also in Figure 4. Of these four quantities, only $d\ell n\ \eta_s/dT$ and to a lesser extent β show marked evidence of critical phenomena. All four show major 'structure' at intermediate compositions $\underline{X} \approx 0.2$-$0.5$ from the chemical association behavior.

Discussion

A quantitative formulation of the chemical model for the TR portion of the absorption and for equilibrium properties begins with the choice of a chain association model for water,[13]

$$A + A_{n-1} \rightleftarrows A_n \quad , \quad K_n = \frac{\delta_n}{\delta_{n-1}\delta_A} \ , \tag{7}$$

where δ_n is the true mole fraction of the species A_n = $(H_2O)_n$,

$$\delta_n = \frac{N_n}{\sum\limits_i N_i} \tag{8}$$

The progression of K_n must follow a simple series to be tractable; K_n = constant = K, or $K_n = K_o r^n$, r = constant are possibilities. The H-bonding of lutidine to water may be described as

$$B + A_n \rightleftharpoons BA_n \ , \ K'_n = \frac{\delta_{Bn}}{\delta_n \delta_B} \ . \qquad (9)$$

Refinements with direct association of two chains and with formation of associations A_nB_m are generally intractable. By postulating the average complexation of lutidine to be with many water molecules, we assure that the relaxation or absorption peaks at a high water/lutidine ratio, as observed. One can solve Eqs. (7) and (9) for the equilibrium concentrations N_α. After assigning volume and enthalpy changes per step, the net $\Delta \underline{V}$ and $\Delta \underline{H}$ of mixing can be computed from these concentrations. These two properties and their temperature dependence are useful criteria for the model. The contribution $G_{\underline{chem}}$ of the reactions to the free energy of mixing $G_{\underline{mix}}$ can be calculated simply as[14]

$$G_{chem} = -RT \ [X_A \ \ell n \ \delta_A + X_B \ \ell n \ \delta_B] \ , \qquad (10)$$

where $\underline{X_A}$, $\underline{X_B}$ are the macroscopic or apparent mole fractions. The condition $\underline{\partial^2 G_{mix}/\partial x_A^2} > 0$ for miscibility maps out the region of phase separation. An extra term $G_{\underline{phys}}$ from 'physical' interactions is necessary[15] to get

$\partial^2 G_{mix}/\partial x_A^2 < 0$, but G_{chem} helps the separation occur and partly determines its location in mole fraction; also, its temperature dependence is crucial to the nature of the consolute point as being upper or lower. Finally, one may assign the forward rate constants k_n, k'_n for reactions (7) and (9) and solve an eigenvalue equation[12] for the relaxation frequencies f_{ci} and relaxation strengths B_i of the 'normal moles' of reaction. This last step is quite difficult in general, especially as a numerical solution must be obtained. The infinite chain of reactions and its analytic form of solution must be retracted.

The CR mechanism contributes to some degree to the static specific heat and compressibility (hence sound velocity) and much to the sound absorption. It has been formulated by Fixman,[2] whose theory is re-examined[3] in paper I. In practice, the forms Eqs. (4) and (5) are used in analyzing absorption data. To represent the data in its composition dependence, the explicit X-dependence of the 'constants' A and C must be known. A and C are known functions of macroscopic quantities as specific heat and density - whose X-dependence is known experimentally to sufficient accuracy - and of the two microscopic parameters ζ and κ^2. ζ is presumably composition-independent, while κ^2 is given by Eq. (26) of paper I,

$$\frac{4\pi a}{\kappa^2} = -\frac{\bar{V}_1}{n_2}\left[\frac{kT}{(\partial\mu_1/\partial n_2)} + \frac{1}{\bar{V}_1}\right] . \qquad (11)$$

The X-dependence on the right is principally in $(\partial\mu_1/\partial n_2)$, for which a Flory-Huggins[16] model may be taken using $(\partial\mu_1/\partial n_2) = (\partial\mu_1/\partial\phi_2)\,(\partial\phi_2/\partial n_2)$. D'Arrigo and Sette[17] in particular have developed this technique, though they made the oversight of taking a factor in the absorption α_{CR} as $(\partial\kappa^2/\partial T)^2$ valid at $X = X_C$, rather than as $(\partial^2\mu_1/\partial n_2\,\partial T)$ $(\partial\kappa^2/\partial T)$. In any event, the total X-, T-, and f-dependence of α/f^2 can presumably be modeled now by Eq. (4) with judicious choice of parameters.

Least squares adjustment of the CR and the TR or chemical parameters to match observed absorptions and equilibrium (including phase diagram) properties is a reasonable expectation. Of course, it is a nonlinear fit requiring iteration, but Andreae, et al.[13] have had modest success in treating a pure TR mechanism in aqueous solutions of nonelectrolytes. In our preliminary work, the qualitative magnitude and X-dependence of α_{TR} were visually estimated from our α_{ex}/f^2 data and several chemical models were tested for plausibility. We became dissatisfied on realizing that phase separation behavior always requires an extra term G_{phys} in G_{mix},[15] making the connection of the α_{TR} and the critical region chemical potential or its relative G_{mix} a very tenuous one. Much of the value of tying the two mechanisms together to analyze all properties is lost. However, we did obtain useful qualitative insight by proceeding to add G_{phys} terms of the form $Ax_B^n x_A$ to force $\partial^2 G_{mix}/\partial x_A^2$ to vanish. Temperature dependence in G_{chem} *alone* then explains the existence of a *lower* consolute point at intermediate mole fraction for small exponents n in G_{phys}, or of an *upper* point at low concentrations forced by a large exponent n. This failure points to deficiencies in the form of G_{chem}, in our understanding of the structure of water and its solutions. To be sure, large H-bonded structures of water and large complexes of water and lutidine exist and such strong H-bonding association seems a general requirement for a lower consolute point. However, the arbitrary distinction of chemical and physical interactions is faulty. Even if elaborate interlocking chemical equilibria are used to describe the former, the ideality of the solution of true chemical species is implicit in the equilibrium constant formulas as in Eqs. (7) and (9). Physical interactions make a continuous transition to chemical bonding and a continuous perturbation from ideality that is difficult to describe in mass action terms. The chemical simplification of the many-body problem fails badly here. This difficulty has not been cited by investigators[18] of other critical systems, since most of these are upper consolutes in which the phase diagram is grounded principally in $G_{\underline{phys}}$ and little TR contribution to α occurs. $G_{\underline{phys}}$ describes an entropy of mixing effect and has an adequate empirical form in the Flory-Huggins[16] theory.

A final and practical barrier to using superposed CR and TR mechanisms to explain the absorption also came to our attention in the generally poor results from use of the composition-dependent Fixman theory. To date, investigators[17,19] have found the theory to predict absorption peaks which are too narrow, at times grossly so, as functions of $\underline{X}$. The necessity of 'classical' thermodynamics of the critical phase diagram and of κ^2 causes the problem. The least-squares fit of Eq. (4), weighting $\alpha_{ex}/\underline{f}^2$ at all compositions equally, would be invalidated. We settle for the lesser information in a least-squares fit to Fixman's parameters from the eight pieces of absorption data at $\underline{X} = X_{\underline{C}}$, consisting of measurements at four frequencies and at two temperatures, $T_{\underline{c}} - 0.92\ \underline{C}$. and $T_{\underline{c}} - 0.12\ \underline{C}$. We obtain the values

$$
\begin{aligned}
A &= 2.2\text{x}10^{-6}\ \text{cm.}^{-1}\ \text{sec.}^{3/4} \\
B &= 201\text{x}10^{-17}\ \text{Np. cm.}^{-1}\ \text{sec.}^{2} \\
C &= 2.0\text{x}10^{2}\ \text{sec.}^{-1/2}\ \text{deg.}^{-1}
\end{aligned}
\qquad (12)
$$

for the best fit as in Table I. Note that Fixman theory is moderately good but gives too sharp an f-dependence and about the right T-dependence. Separate fits for the two temperatures use three parameters for four points, but serve to show that the theory is strained, as the B values become large and unphysically negative. The B value for the eight-point fit, on the other hand, is very reasonable in light of the size of the TR peak at $X \approx 0.1$. Final reduction of the A, C values to estimates of the Debye persistence length ℓ and the friction constant ζ was made with the correction noted after Eq. (46) in paper (I), and it yields

$$
\begin{aligned}
\ell &= 9.0\ \text{Å} \\
\zeta &= 0.32\ \text{x}\ 10^{13}\text{sec.}^{-1}\ ,
\end{aligned}
\qquad (13)
$$

in the same range as for other systems similarly corrected. The value of the correlation length κ^{-1} at T_c - 0.5 C. is, from Eq. (39) of paper I,

$$\kappa^{-1} \approx 91\ \text{Å} \qquad (14)$$

compared to an estimated 100-200 Å from light scattering data in our laboratory.[20] Our final quantitative work with Fixman theory is calculating the ratio of the excess absorptions from the temperature and pressure perturbations of the sound wave. Only the former is included in the theory as originally developed. The second pressure term was suggested by Puls[19] and is formulated in our paper I. The result, a pressure contribution only 0.4% of the temperature term, supports Fixman's choice of the dominant perturbation.

We can extract more information of a qualitative nature from $\alpha_{ex}/\underline{f}^2$. Earlier we noted that the $\underline{f}$-dependence is expected to lie principally in the CR mechanism. The appearance of significant $\underline{f}$-dependence to $\underline{X} \approx \frac{1}{2}\underline{X_c}$ and to $X \approx 2\underline{X_c}$ indicates a fair extent for CR. The $\underline{T}$-dependence of $\alpha_{ex}/\underline{f}^2$ has more detail. Near $\underline{X} = 1.0$, it is positive as expected for internal vibrational relaxation of pure lutidine.[21a] At the intermediate composition $\underline{X} = 0.3042$, it dips slightly negative, as expected[21b] for thermal relaxation of lutidine/water associations. It is large and positive for the remainder of the composition range. The magnitude is the same at both peaks in $\alpha_{ex}/\underline{f}^2$, indicating either a larger extent for CR than hinted by the $\underline{f}$-dependence, or a change to positive $\underline{T}$-dependence for

TR in this range. Now the 'definition' of the CR peak at $\underline{X} = \underline{X_c}$ is good only at $\underline{f}$ = 4.5 MHz for $\underline{T} = \underline{T_c}$ - 0.92 $\underline{C}$. This suggests the CR mechanism is at least as restricted as the $\underline{f}$-dependence indicates. Thus the TR temperature coefficient seems to undergo a sign reversal not very far down its shoulder in a composition profile, which points once again to complexity in the chemical behavior.

The sound velocity β showed no clear dispersion with frequency in our most reliable measurements. The 4.5 MHz values show nontrivial composition dependence. At low lutidine concentrations β rises rapidly with $\underline{X}$, due to breaking down of water structure (chain-length) that causes a decrease in compressibility.[13] Around $\underline{X}$ = 0.15 and just beyond the composition of peak TR absorption, β turns downward. The trend is not smooth, for the region near $\underline{X} = \underline{X_c}$ forms a step of increased velocity. Everywhere the temperature derivative is slightly negative or vanishing. This corresponds in the critical region to the expected increase in compressibility on nearing the critical state. In regions dominated by the chemical phenomena, the positive temperature coefficient of compressibility shows that the simple reduction of water structure breaking (by the decrease of chemical association) more than counteracts the decrease in the chemical contribution to the compressibility (from the same cause).

The excess volume $\Delta \underline{V}$ shows a broad minimum near $\underline{X} = 0.5$. This is probably due to peaking here of the chemical association as measured by greatest reduction in water chain length. Similarly, the shear viscosity peaks near $\underline{X} = 0.3$, and by Eyring's[22] theory of viscosity this is roughly the peak of the heat of vaporization. Another measure of complexation, involving the enthalpy changes $\underline{\Delta H_i}$ of the chemical steps, must be largest here. The temperature coefficient of the shear viscosity, $d\ell n\ \eta_s/dT$, has been estimated from a fit of the η_s data to the form

$$\eta = Ae^{-E/T}\ \left(+\ \frac{B}{|T-T_c|^{1/2}}\ \text{in critical region}\right). \qquad (15)$$

It is uniformly negative except for a sharp positive-going peak at $\underline{X} = \underline{X_c}$. Critical phenomena contributions appear as well-localized and as strong here as in absorption.

Table I. Comparison of experimental absorption data with best fit from Fixman theory at the critical composition $X = X_c$.

	f(MHz.)	$\alpha_{ex}/f^2 x 10^{17}$,Np. cm.$^{-1}$sec.^{2} Experimental	Best theoretical fit
$T=T_c-0.92$ C.	4.5	557	573
	7.5	465	406
	10.5	327	338
	13.5	262	303
$T=T_c-0.12$ C.	4.5	613	641
	7.5	498	435
	10.5	358	355
	13.5	285	314

Acknowledgments

We would like to thank William C. Hocker for helping with the experimental measurements. We are grateful to George Griffith and his staff for expert design and construction of sections of the apparatus, and to John Yehle for help with electronics problems. Hollis Reamer is due thanks for many suggestions on experimental technique.

References

1. K. F. Herzfeld and T. A. Litovitz, Absorption and Dispersion of Ultrasonic Waves (Academic Press: New York, 1959), Sections 27-29; A. B. Bhatia, Ultrasonic Absorption (Clarendon Press: Oxford, 1967), Sections 9.4, 9.5.

2. M. Fixman, J. Chem. Phys. **36**, 1961 (1962).

3. V. Gutschick and C. J. Pings, J. Chem. Phys. xx, xxxx (1971).

4. J. D. Cox and E. F. G. Herington, Trans. Faraday Soc. **52**, 926 (1956).

5. a) J. H. Andreae, R. Bass, E. L. Heasell, and J. Lamb, Acustica **8**, 131 (1958);
   b) A. V. Anantaraman, A. B. Walters, P. D. Edmonds, and C. J. Pings, J. Chem. Phys. **44**, 2651 (1966).

6. R. Bass, J. Acoust. Soc. Am. **30**, 602 (1958). There is some experimental evidence and qualitative theoretical argument that Bass' corrections are not adequate when they reach 25-50% or more of the total apparent absorption. See E. F. Carome, J. M. Witting, and P. A. Fleury, J. Acoust. Soc. Am. **33**, 1417 (1961). Our data were never corrected more than 20% even at the lowest frequencies and lowest-absorbing compositions. Typically, our corrections were of the order of 1%, and not more than 5% at the lowest frequency in the critical region. Our empirical correction for mode conversion at the two lowest frequencies is about as large as for diffraction, at the lowest frequency. No assessment of its adequacy is available.

7. D. Sette, Nuovo Cimento Suppl. **6**, 1 (1949).

8. Full numerical tables of the absorption coefficients may be obtained from ADI Auxiliary Publication Project, Photoduplication Service, Library of Congress, Washington, D.C., by requesting Document No. XXXXX and remitting in advance $X.XX for photoprints or $X.XX for 35-mm microfilm. Make checks or money orders payable to Chief, Photoduplication Service, Library of Congress.

9. See, for example, Bhatia, op. cit., Secs. 4.3, 4.4; note that his α is $\alpha\lambda$ in our terms, the absorption per wavelength.

10. A. E. Brown and E. G. Richardson, Phil. Mag. 4, 705 (1959); A. E. Brown, Acustica **18**, 169 (1967).

11. Herzfeld and Litovitz, *op. cit.*, Secs. 99, 117.

12. The generalization of relaxation of chemical equilibrium as in Ref. 1 to cases of more than one reaction is treated by M. Eigen and L. de Maeyer, *Techniques of Organic Chemistry*, ed. Weissberger, et al. (J. Wiley and Sons, Inc.: New York, 1962), Vol. VIII, Part 2; see esp. Eq. (II. 3. 90b) in the section on sound absorption.

13. J. H. Andreae, P. D. Edmonds, and J. F. McKellar, Acustica **15**, 74 (1965).

14. J. M. Prausnitz, *Molecular Thermodynamics of Fluid-Phase Equilibria* (Prentice-Hall, Inc.: Englewood Cliffs, N. J., 1969), Eq. (7.15-13); γ_i chosen as δ_i for ideal solution.

15. J. S. Rowlinson, *Liquids and Liquid Mixtures* (Butterworths Publ.: London, 1959) p. 181; I. Prigogine and R. Defay (transl. D. H. Everett), *Chemical Thermo dynamics* (Longmans, Green and Co., Ltd.; London, 1954), Ch. XXVI, Sec. 8.

16. J. H. Hildebrand and R. L. Scott, *Solubility of Nonelectrolytes* (Reinhold Publ. Corp.: New York, 1950).

17. G. D'Arrigo and D. Sette, J. Chem. Phys. **48**, 691 (1968).

18. See the 'Discussion and Redevelopment' section of Ref. 3 for a recounting of earlier experiments as analyzed by Fixman theory plus a Flory-Huggins form for the phase behavior.

19. M. P. Puls, Thesis, McMaster Univ., May, 1970.

20. E. Gulari, unpublished work.

21. a) Herzfeld and Litovitz, *op. cit.*, p.356; b) p.510.

22. J. O. Hirschfelder, C. F. Curtiss, and R. B. Bird, *Molecular Theory of Gases and Liquids* (J. Wiley and Sons, Inc.: New York, 1954), Ch. 9, Sec. 2a.

Figure Captions

Fig. 1 - Excess absorption of sound at $T = T_c - 0.92$ C. for four frequencies.

Fig. 2 - Excess absorption of sound at $T = T_c - 0.12$ C.

Fig. 3 - Excess absorption of sound at $T = T_c + 1.08$ C. ($T_c + 0.28$ C. for solid points).

Fig. 4 - Sound velocity and excess volume of mixing. Velocity is averaged over two or three temperatures near T_c and qualitative trend with temperature $d\beta/dT$ is indicated by +, -, or 0 under data point. Excess volume is measured at $T = 32$ C. $= T_c - 1.57$ C.

Fig. 5 - Shear viscosity η_s and its logarithmic temperature derivative, both at $T = T_c - 0.37$ C. See Eq. (15).

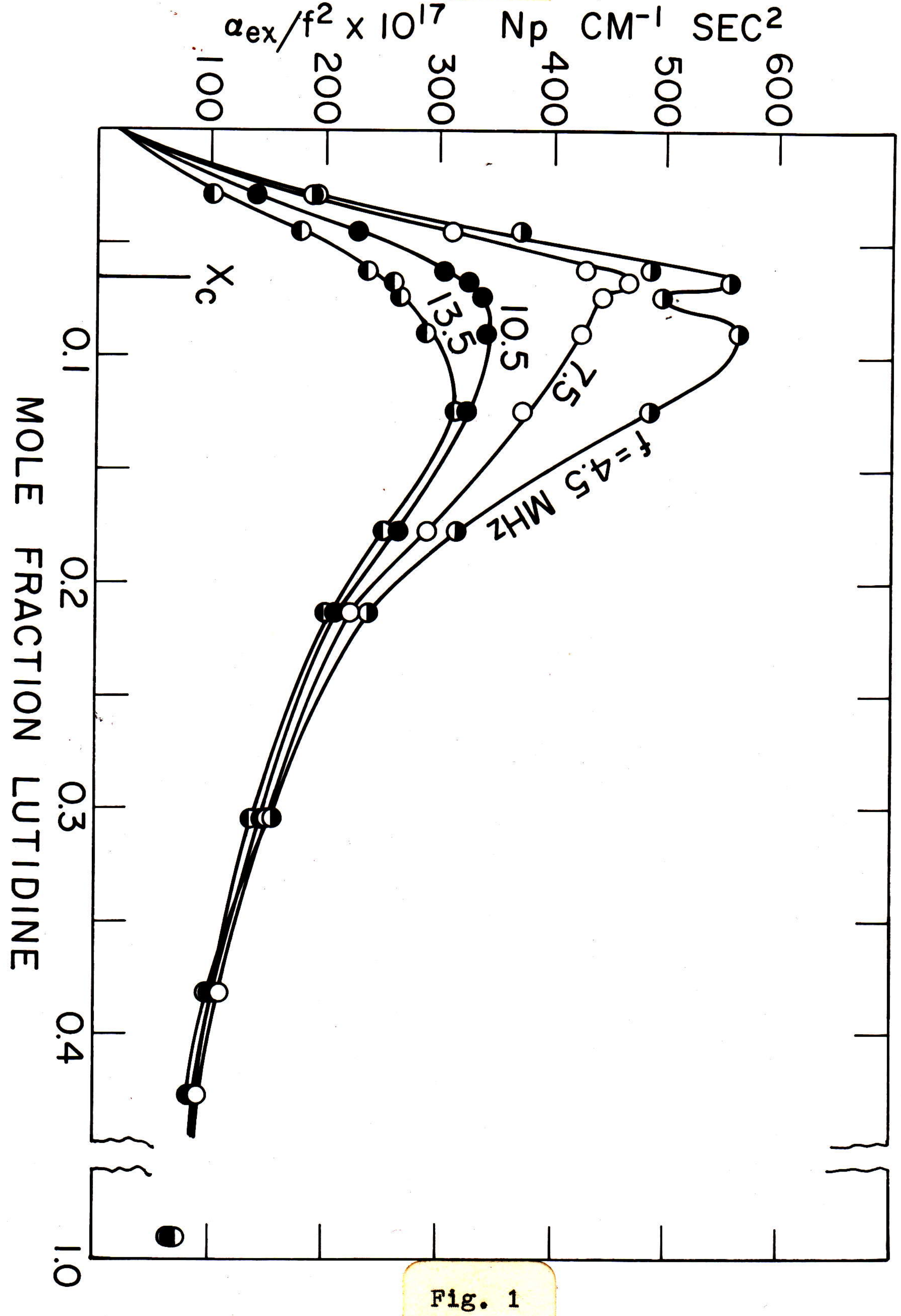
$\alpha_{ex}/f^2 \times 10^{17}$ Np CM^{-1} SEC^2
100
200
300
400
500
600
MOLE FRACTION LUTIDINE
0.1
0.2
0.3
0.4
1.0
X_c
13.5
10.5
7.5
f=4.5 MHz

Fig. 1

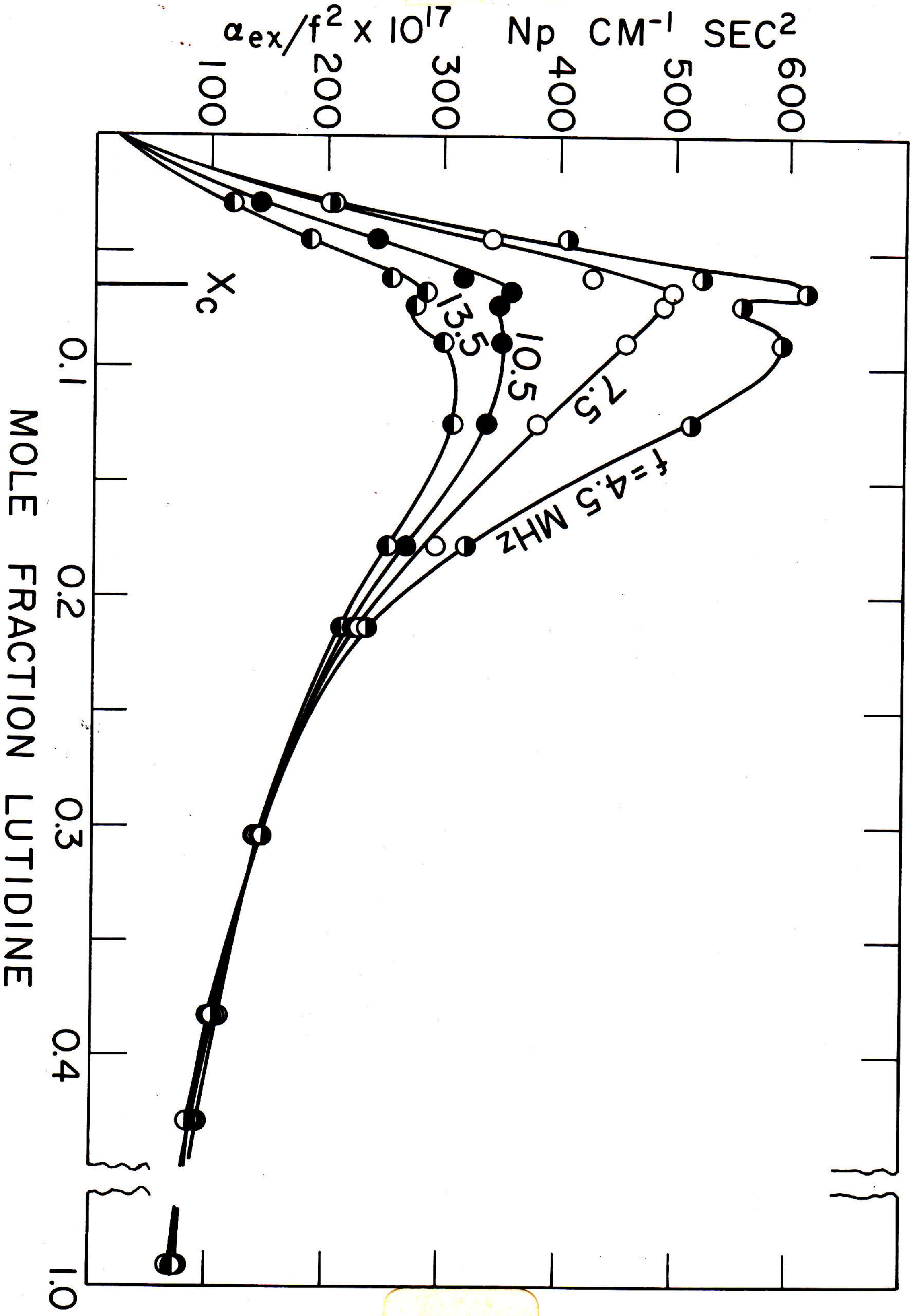
αex/f² x 10¹⁷ Np CM⁻¹ SEC²
100
200
300
400
500
600
MOLE FRACTION LUTIDINE
0.1
0.2
0.3
0.4
1.0
Xc
13.5
10.5
7.5
f=4.5 MHz

Fig. 2

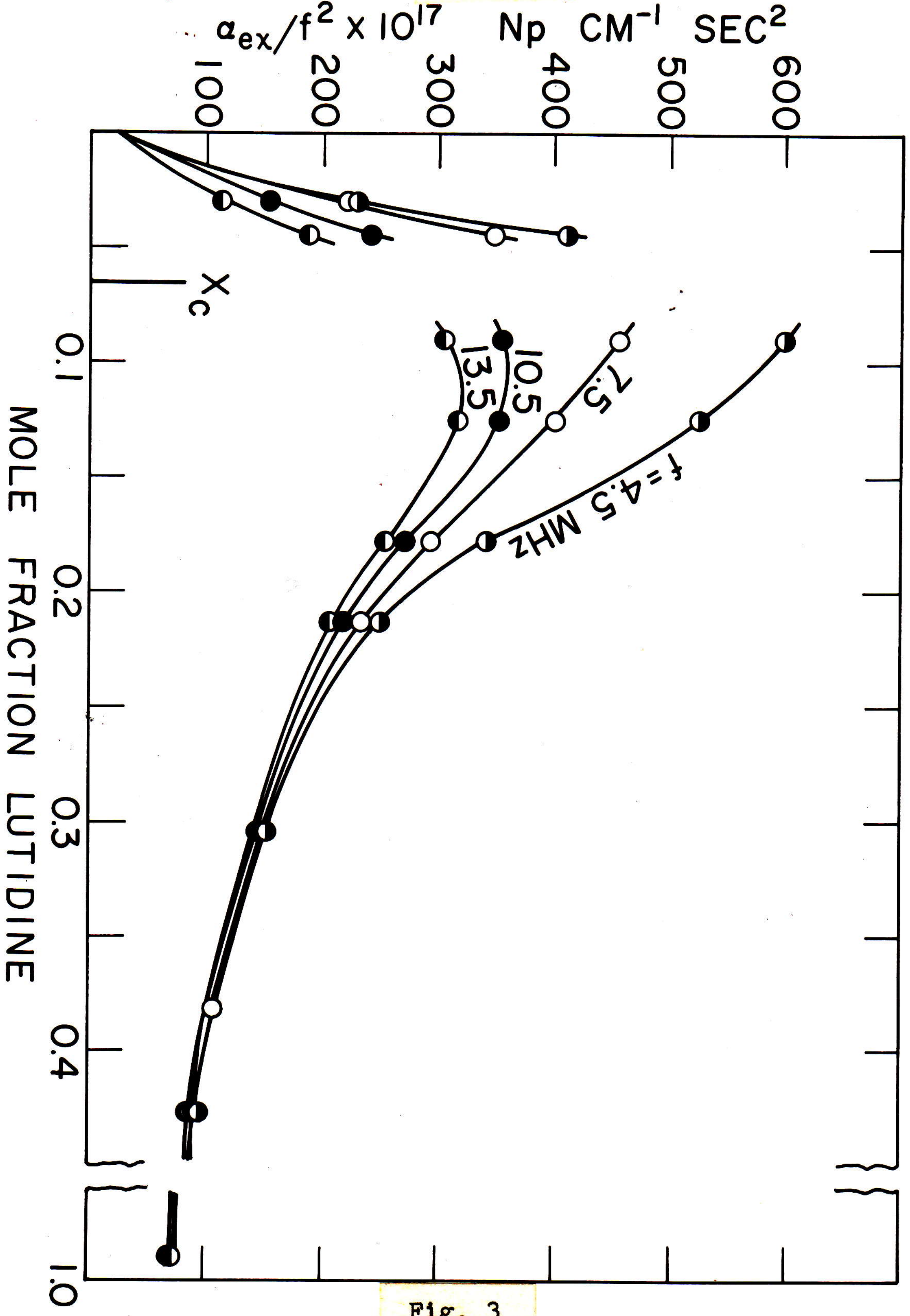
$\alpha_{ex}/f^2 \times 10^{17}$ Np CM^{-1} SEC^2
100
200
300
400
500
600
X_c
0.1
0.2
0.3
0.4
1.0
MOLE FRACTION LUTIDINE
f=4.5 MHz
7.5
10.5
13.5

Fig. 3

Appendix I. Experimental Apparatus

Our ultrasonic cell is a slight modification of that of Andreae, et al.[1] It was constructed principally by P. D. Edmonds and A. V. Anantaraman for earlier binary liquid studies in this laboratory[2], with special care in design for the close temperature control required near critical states. We have further modified it for better temperature control and homogeneity, prevention of bulk composition changes from air contact, and improved electronic stability. The basic sample cell is a 300 ml. thin-walled copper cylinder brazed to a brass base and surrounded by a circulating water jacket on the same base providing temperature control. The sample liquid has a free surface and is covered on top by a screw-on plate similar to the base. Coaxial upper and lower ultrasonic delay rods, of low fixed losses, project into the liquid through holes in the base and cover to conduct the sound from transducers to the liquid gap. This arrangement keeps the transducers out of the corrosive and somewhat conductive solution. Extra fittings on the cell provide for stirring and for vapor venting (through a buffer solution). In manner of sound propagation, the apparatus is described as a pulsed, variable path, single pass cell. Short sound pulses, converted from RF pulses by a transducer, traverse the acoustical path in the liquid between the delay rods. The attenuated pulses are reconverted to electrical signals by a similar transducer at the end of the lower rod, amplified (in a tuned preamp for lower noise), and displayed on a CRO screen. The path is varied by moving the upper rod up or down, and the change in received signal amplitude is observed and eventually reduced to a linear attenuation α. Similarly, the change in received signal delay is converted to a sound velocity β.

The pulse technique contrasts with the interferometric methods employing continuous standing waves and either electromechanical (transducer) or optical detection[3]. Continuous wave methods heat the sample more and are therefore less desirable in the critical region. Our method also contrasts with the pulsed double pass, where a reflector returns the attentuated pulse to the same transducer which generated it. While this guarantees a transducer match, it requires sophisticated fast switching between electrical transmitting and receiving circuitry and has trouble with moderately long pulse trains at short acoustical paths. Fixed path pulsed methods[2] are also in use for samples confined under unusual conditions where sealing of the moveable delay rod or the disturbances induced by its motion cause difficulties. Absolute signal levels must be measured, which is difficult. Pinkerton[4] discusses the best implementation of the pulse methods.

We used pycnometers and an auxiliary temperature bath to measure densities of solutions at representative compositions, and the bath with a viscometer to measure shear viscosities. The densities were used to compute excess volumes of mixing and also to establish a $\rho \leftrightarrow \underline{X}$ curve for identifying solutions by density, after making them up quickly by volume. The exact locus of the critical point $(\underline{X}_c, \underline{T}_c)$ was examined in more detail to ensure that the states we investigated for ultrasonic and viscous behavior were accurately located relative to the critical point, irrespective of absolute errors in $\underline{X}_c$ and $\underline{T}_c$. The ultrasonic cell and auxiliary equipment were extensively calibrated and tested for operating problems, and reliable operating procedures were set up. We recount below the detailed construction of the apparatus and the underlying design considerations. At the end we tabulate the equipment specifications and list the suppliers. Later appendices describe the test and calibrations, and finally the results.

<u>CELL</u>: Figure 1 is a sketch of the important mechanical parts of our apparatus. To give scale, we note that the delay rods are 1" in diameter and 6" long. The walls of the cell are of 23 gauge copper formed into a cylinder of 3½" inside diameter by 2-3/4" tall. The general dimensions are dictated by the magnitude of the absorptions expected and the usable frequencies. A range of about 10-12 db in attenuation is conveniently measured by our comparison pulse technique (discussed shortly) using a precision attenuator in the comparison pulse circuit along with visual matching.

A frequency range of a factor of four or so is desirable, to test the frequency dependence of absorption predicted by various theories. To minimize diffraction losses, the lowest frequency should have a wavelength (in the sample material) less than around 0.04 of the diameter of the transducer. At the same time, the transducer should be moderately thick for mechanical strength, while it should be used near its fundamental frequency which is inversely proportional to its thickness. At a modest diameter of 1¼" (larger than the delay rod), a thickness of 0.075" is reasonable, giving it a fundamental of 1.5 MHz. Odd harmonics are easily excited, so that a range of 4.5-13.5 MHz is practical for both the transducer and the pulse generator; at 1.5 MHz. we have too great a diffraction loss. This *f*-range is in the lower range of thermal relaxation frequencies for mixtures[5], so that we might touch on these interesting phenomena as well as critical relaxation. The expected α/f^2 values are of the order of 10^{-14} Neper cm.$^{-1}$ sec.^{2}, several tens or hundreds of times the classical losses. One Neper, abbreviated Np., is equivalent to an attenuation of amplitude by a factor of *e*, and hence to 8.686 db of *power*. Thus α values of 0.2-2 db per cm. are expected and a delay rod travel of 5-6 cm. is desirable.

Given the acoustical path dimensions, the remaining design considerations for the cell center on making the cell walls sufficiently distant from the beam to prevent echoes, achieving good sample temperature control, homogeneity and purity, and insuring accurate and stable mechanical alignment of the delay rods. Drawings 50023-1,-2, and -3 on file in the Chemical Engineering drafting lay out the original design. A cell diameter several times the delay rod's loses the echoes yet leaves possible good thermal contact (with stirring) of sample with circulating jacket. Corrosion protection was afforded in the original design by nickel plating, which is sufficient in the nitrobenzene-isooctane system but not for lutidine/water. Lutidine, a nitrogen heterocycle, is a powerful copper complexing agent. It presented us with severe corrosion problems (notebook *5072*: 50,98,102ff.,127; *5090*: 114) until gold and later silver platings were applied (see notebook *5072*: 127; *5090*: 79,116-23,124-5, es½. 130-36).

Temperature-control water for the circulating jacket is drawn from a large-capacity (30 liter) bath thermostatted by a Sargent S-84805 controller. Control within 0.03 C. is achieved in both bath and cell (notebook *5072*: 8, 19), with a loss of 0.01 C. in temperature on the way to the cell via thick rubber tubing. A small submersible 1/30 hp. centrifugal pump does the lifting job. The outer circulating jacket is of no critical dimensions. Originally, it did not encompass the cell bottom--only the sides, while heat losses from the bottom set up convection currents upsetting signal stability (notebook *5072*; 104 ff.). We added a false bottom (notebook 5072: 109) and connected it to the rest of the jacket with a number of large drill holes. Even this was not sufficient (notebook 5090: 79) and we eventually enclosed the whole apparatus in a Lucite box (notebook 5090: 80-82). Cables, the micrometer handle, the stirrer string, and two air temperature thermometers entered through ports; jacket hoses entered through the bottom (the apparatus cabinet) as before. A small heater-blower controlled by one of the thermometers maintained a preset air temperature within 0.2 C. Snap-out Lucite panels with aluminum borders for screw fastening allowed easy manual access to the cell.

The cell is made to seal on the lower rod simply by resting upon the rod's taper. Both rod and hole must be precisely machined (drawing 50012). In addition, a thin plastic sleeve or shim must be used between rod and cell; we eventually settled on a Teflon cone made by the shop. The cell must not be too heavy to be supported by the delay rod without damage or a bending misalignment.

The last main part of the cell is the upper plate (drawing 50023-1) which serves to contain the pressurized circulating water in the outer jacket and also to shield the sample from the ambient air in large part. To accomplish the former task, the cover plate is grooved and fitted with a large nylon O-ring (½" wide, 1/16" thick) of median diameter equal to the cell proper diameter. This seals by compression, aided by a disposable ring of Teflon tape draped over the cell walls, upon screwing the plate to the outer flange of the jacket. To shield the liquid from the air, the plate's center hole must be only minimally larger than the upper delay rod. The original design left an annulus of about ¼" around the rod, large enough to allow a lot of evaporation, and also incorporated an ineffective 8-vaned coaxial stirrer. These two defects are corrected by the auxiliary fittings discussed shortly.

DELAY RODS AND TRANSDUCERS: are the other main concern. The rods must have low absorption loss at the highest frequencies, and be strong and elastic. Fused silica is excellent, at least for the upper rod, as it has an absorption $\alpha = (3\times10^{-10}f + 1.9\times10^{-17}f^2)$ db cm.$^{-1}$ (ref. 6a). Silica was also used in the lower rod originally, but it chips too easily under stress. Duralumin alloy, of similar low loss[6b], are a better choice. The upper rod must be carried on a micrometer-mounted arm (drawing 50013-1) and thus it and its transducer assembly must be light. The rod must be long enough beyond the transducer housing and arm clamp to project through the thickness of the cell cover plate and through the vapor space into the liquid 6-8 cm. A length of 6" is sufficient. The edges of the rod are beveled to reduce the chipping hazard in handling. The faces have a finish of about 1/20 th of the shortest wavelength (in the liquid) to be used, to prevent surface scattering of the signal at the rod-liquid interface, and to assure good acoustical contact at the transducer end. The face should also be perpendicular to the axis within an angle θ such that R sin θ is again about 1/20 th the wavelength, to minimize refraction errors. The supplier, Englehard Industries, automatically finishes the rods to one wavelength of light and an alignment of 1" of arc, which is adequate up to 200 MHz. in ultrasonics. Somewhat larger diameter irregularities are tolerable. The final design is given in drawings 50012,-1 (Edmonds) and 60037 (our work), also on file. The lower rod must be held securely in a wide base attached to the micrometer. A collet design is given in drawings 50013, -1, and -2, with trimming screws to to align the planes of the two delay rods. The main micrometer assembly pivots on a vertical post from its base to bring the rods into coaxiality. A lower rod length of 6" is also sufficient. A Gaertner micrometer model M342 was chosen to carry the tubular arm which clamps onto the upper rod (drawing 50013 -1). The required micrometer travel accuracies and precision must restrict to a few tenths of a percent the error over the shortest distance in which one db attenuation occurs. The Gaertner's implicit specifications of better than 0.005 mm. satisfy this readily.

X-cut quartz transducers are excellent[3,6] for their high signal purity and low loss (high Q-value, though this also means low conversion efficiency), and atmospheric stability. They must be matched to within about one-quarter of their frequency bandwidth in circuit. Gold platings on both sides form the electrodes for applying the RF signal. Transducer housings (drawings 50012,50013-2) position each transducer against the delay rods for acoustical and electrical contact. Electrical contact to the upper side of the transducer is made through a copper leaf pressed onto the face by a spring inside the housing. The spring also helps the acoustical contact, which is completed by a film of silicone grease between rod and transducer <u>not</u> covering the entire surface. The ungreased annulus forms an electrical contact of the lower transducer face and delay rod (in the case of the silica rod, there is a Cr-Ni or Ag plating over the face and one inch down the rod sides, maximum resistance 10Ω between any two points). The delay rod in turn contacts the grounded transducer housing. In use the delay rods are pressed into their housings far enough to lift the oversize (1¼") transducers a fraction of an inch from their resting positons over the rod holes in the housings. A collet fitting on each housing grips the delay rod and maintains the pressure. Standard coaxial cables with low-loss polymer dielectric carry the signals in and out to the external electronics.

<u>OTHER CELL ACCESORIES</u>: There are three auxiliary fittings on the cell. First is an evaporation buffer (notebook <u>5072</u>: 62) added for our work, mounted on the cover plate. It is needed because the vapor volume above the

sample changes as the delay rod moves. Makeup air flow is routed (bubbled) through a smaller sample of liquid, about 5 ml., which undergoes sacrificial composition changes by evaporation and water pickup, protecting the bulk sample composition. The tubing from the buffer volume enters the cell volume through the second accessory, a short length of threaded pipe brazed to the cover plate and encircling the upper delay rod. A thick Teflon ring fits in a collar screwing onto the pipe, to seal closely but without binding against the delay rod. The third fitting is our ring stirrer, replacing the old vaned stirrer of the original design. A horizontal, flat, 16 gauge stainless steel ring 3" O.D. by 2¼" I.D. travels up and down in the sample to provide fast and efficient mixing.(notebook 5072: 107). Its vertical pushrod emerges from the cover plate through a bushing. It ties to a string, the other end of which attaches to a flywheel on a small 57 RPM motor to provide reciprocating motion; the stirrer falls by gravity.

ELECTRONICS: Figure 2 gives the electronic configuration needed for the pulse technique. A Chesapeake U-100 RF generator puts out a continuous series of shaped 8 μsec. pulses to the upper transducer, through a transformer (impedance matching box; notebook 5031: 17, 20, P. D. Edmonds) for improved signal transfer. After passing through the sample and being reconverted to an electrical signal at the lower transducer, the received pulse passes through a tuned preamp (Arenberg PA-620L) powered by a regulated HV supply (HP 712B), and is displayed on a CRO (Tektronix 547, with 1A1 dual-trace plug-in). The sample's attenuation of the signal as a function of liquid path length is observed visually on the CRO and measured by reference to a comparison signal which can be attenuated in precise steps. At some initial path length or micrometer height, the received signal and the comparison signal are displayed superposed on the CRO with their amplitudes adjusted to match at the peaks of their envelopes. The comparison signal is attenuated or deattenuated one fixed step (one db, with our attenuator) and the path length is changed to bring the pulses into superposition again. This is repeated until one runs out of micrometer travel or attenuator steps. The data points of relative attenuation as a function of height, $a(h)$, are least-squares fit to the form $a = \alpha \overset{h}{x} + b$ to get the linear absorption coefficient α . In practice, theoretical diffraction losses are first subtracted from $a(h)$. The lower half of the electronics schematic is concerned with the display of the comparison pulse. Part of the initiating pulse shaping the RF output pulse of the Chesapeake is taken off as a trigger signal. This is subsequently reshaped into a square wave of very stable height and adjustable duration by the Tektronix 162 and 163 units. This square wave modulates the RF output of the highly stable reference signal generator, an HP 606A. The precision, frequency-compensated

0-12 db attenuator (HP 355 C) passes the signal out to the second channel of the CRO. The use of separate CRO channels for received and comparison pulses eliminates the problems of impedance changes and mixing nonlinearity. It also facilitates use of the variable time delay on the second channel to bring the signals into superposition--especially for velocity measurements discussed shortly. The only critical parameters in the setup not related to stability are the 50 ohm impedances which must be presented to the input and output of the attenuator for it to give calibrated attenuations. The HP 606A has an output impedance of 50Ω; the scope channel input must be terminated by a frequency-compensated 50Ω dummy load (Tektronix part no. 011-0049-00); and the generator-attenuator-dummy load interconnections must be made with 50Ω cable. These considerations were overlooked in the original electronic design.

Of course, the preamp in the received channel must be linear and noise free. The overall signal levels are chosen as the smallest for an acceptable signal-to-noise ratio at the CRO (say, 10 db) at the highest attenuation at the preamp's frequency of least gain. For our system, a 300V peak-to-peak signal at the upper transducer is satisfactory. A pulse duty of less than one percent insures low sample heating; the 8 μsec. pulses repeat on the average every msec. The pulses must be long enough to contain about 50 RF cycles minimum to insure good spectral purity, and they must similarly be well-shaped and smooth.

Sound velocities are measured from the received signal delay as a function of liquid path. Initially the received signal's leading edge is aligned with one fiduciary line on the CRO screen (the peak is flat and hard to locate). As the path length is changed, the variable delay on the CRO necessary to restore the display is observed. A least-squares fit of delay to height yields the sonic velocity directly. There are some difficulties with the technique, as the signal amplitude varies with liquid path and hence in discernible shape. Limited careful checks in which one particular RF cycle was tediously followed rather than the envelope edge indicate that only the least-absorbed 4.5 MHz. signal is suitable for the simpler leading-edge type of measurement.

AUXILIARY EQUIPMENT: As mentioned above, we require an apparatus to determine densities of solutions, either for establishing initial $\rho \leftrightarrow \underline{X}$ correlations or for identifying compositions of aliquots taken from samples being used in ultrasonic or viscosity measurements. We use glass pycnometers hand-blown from marked small-bore tubing. As a result of the marking, they have calibrated divisions on the neck for reading and interpolating the liquid volumes. They also have caps for stopping evaporation. The caps must be placed on carefully to avoid slightly pressurizing the contents, as the thin pycnometer bottoms bulge easily. They are filled using ground-glass syringes fitted with long 17 gauge or finer stainless steel needles.

The pycnometers are thermostatted in a Tamson TV40 water bath of 40 liter controlled volume. The bath controls within 0.005 C. over an hour with a variation over the volume of 0.005 C. To achieve this accuracy, the bath requires a regulated flow of cooling water of fairly stable temperature, with flow rate and temperature adjusted to induce the proper cooling/heating cycle. Cooling water is supplied by a Tamson T3 water circulator, itself cooled by either tap water or the probe of a Tamson PBC-5 portable refrigeration unit.

Temperatures were commonly observed visually on Princo -10 to +100 C. or -10 to +50 C. glass thermometers. Readings could be interpolated and reproduced to a little worse than 0.01 C. A platinum resistance thermometer (Leeds and Northrup ser. 676711; notebook <u>5090</u>: 145 ff.) was used in conjunction with a potentiometer to observe the bath fluctuations, to calibrate the glass thermometers, and to closely resolve the critical point. These tests and calibrations are described in a later Appendix.

The pycnometer masses, dry and filled, were measured on an analytical chain balance (Weston Bros. type BB, ser. 35973; weights: Ch. E. no. 20187) to o.1 mg. after cleaning and drying their exterior surfaces with reagent acetone. Reagent acetone was also used to clean and dry their interiors, along with dry air blown in through stainless steel needles. The balance was also used in making up flasks of solutions by weight for the initial $\rho \longleftrightarrow \underline{X}$ studies.

Shear viscosities were determined in an Ostwald-Cannon-Fenske viscometer, of the bent-U design with two calibrated bulbs on the capillary arm of the U separated by a neck marked with a reference line. Viscometer operation and calibration is discussed in NBS Monograph no. 55. The viscometer was held in the Tamson bath by an array of clamps and aligned visually with a plumb line. For proper temperature control the viscometer must be almost fully submerged. Then to impeded water vapor and/or air from circulating in the viscometer vapor space, we led plastic tubing from the arm ends to the outside air. Flow times were recorded with a synchronous electric timer resolving to 0.01 sec. operated by a snap switch. The viscometer was cleaned originally with chromic acid cleaning solution briefly, and routinely with reagent acetone.

CHEMICALS: 100 gm. bottles of Matheson, Coleman, and Bell 99% purity lutidine were combined into 500-1000 ml. lots, dried by refluxing over BaO, and distilled (notebook 5072: 19,68,104,113; 5090: 28,115). Occasional water determinations in the stored, distilled lutidine by titration with Karl Fischer reagent showed contents of 0.04% typically. Better purification could be obtained by gas chromatography, fractional crystallization, or zone-refining the solid, but these are too difficult. Laboratory distilled water was the other component of the critical mixtures and also served as one of the viscometer calibrating fluids. Metal ion assays performed incidental to cell corrosion tests showed traces of Sn ions but no other common metal contaminants. Baker reagent acetone was used in cleaning and also for viscometer calibration. A total ultrasonic calibration, to be described later, was run on Mallinckrodt thiophene-free analytical reagent benzene, titrating as less than 0.12 mole 5 water (notebook 5096: 20,34).

Lutidine/water samples for viscosity, $\rho \leftrightarrow \underline{X}$ studies, and ultrasonics were all disjoint. The large amount of lutidine used in any one ultrasonics sample necessitated several consecutive reuses of the same sample, diluted appropriately each time. Upon long storage the solutions tended to discolor but critical properties--at least $\underline{T_c}$--seem unaffected.

SUPPLIERS

Chesapeake Instrument Co.
Shadyside, Md.

U-100 signal generator (ser. 118)

- -500 W instantaneous peak into 100Ω resistive load; adjustable.
- -0.9-200MHz. with 12 plug-in coils
- -rise time 0.5 μsec.
- -pulse width 1, 1.5, or 6 μsec. nominal
- -internally or externally triggered; 100V
- -pulse repetition rate, internal trigger: 50-7000 Hz.

Arenberg Ultrasonic Laboratory, Inc.
94 Green Street
Jamaica Plain, Mass. 02130

PA-620L preamp (ser. SN 241)

-gain: dependent on freq. and bandwidth; approx. 35 db min.
-Input impedance 93-15,000Ω; output 2.7kΩ, capacitatively coupled
-0.1-17 MHz.
-has instruction manual on file

Hewlett-Packard
275 Page Mill Road
Palo Alto, Calif.

712B regulated DC power supply (ser. 002-04783)

-0-500 out, 200 ma. max. load; also -300V, 50 ma.; 6.3V AC CT, 10 A. (unreg.); etc.
-less than 50 mv. change on 500V line, no load to full load
-less than ±100 mv. change for ± 10% line in.
-less than 500μv ripple
-internal impedance at full load 0.1Ω in series with 25μH
-current metering; overload protection

606A signal generator (ser. 038-03448)

-(extensive spec sheet)
-50kHz.-65 MHz. in 6 bands; freg. acc. within 1%
-calibration within 0.01% (BFO), 0-50 C.
-RF output 0.1μv-3V continuously adjustable, into 50 resistive load
-output accuracy with change of vernier ±1 db
-freq. response ± 1 db over the entire freq. band range at any setting of output
-output impedance 50Ω; SWR 1.1 on 3V range; less than 1.1 on 1 and 3V ranges to 20 MHz.
-spurious harmonic output < 3%
-continuously adjustable amplitude modulation 0-100%, constant within ±½ db over full range of carrier freq. and output level; DC to 20 kHz. bandwidth
-envelope distortion < 1% at 30% modulation
-incidental FM < 0.0025% or 100 Hz. (larger) on 1V and lower ranges
-spurious FM < 0.001% or ± 20 Hz.
-spurious AM: hum and noise -70 db

-freq. drift: 1V and lower ranges,< 0.005% or 5 Hz. for 10 min. period after warmup or restabilization at freq. of use

355 C attenuator (ser. 219-00194)

-0-12 db in 1 db steps, ± 0.05 db
-0-1000 MHz. compensation
-0.5 W max. dissipation
-50Ω in and out

Tektronix, Inc.
S. W. Millikan Way
P.O. Box 500
Beaverton, Oregon

547 oscilloscope (ser. 006668)

-(extensive spec sheet and manual)
-sweep rates 0.1 μsec./cm. to 5 sec./cm. in 24 calibrated steps, ± 2%; uncalibrated vernier to 0.4 of rate
-sweep magnification 2X, 5X, and 10X, ± 5%
-trigger source, coupling, level all adjust.
-time-delay on sweep 0.1 μsec. to 50 sec., ± 1% of indicated delay, ± 2 minor divisions of multiplier 50 μsec.-50 sec.; incremental delay accuracy ± 2 minor divisions; jitter < 0.005%
-horizontal deflection continuously variable 0.1 V/cm. to 10 V/cm.; DC-400 kHz. (3 db)
-input 1 MΩ, shunted by 55 pF.
-has internal amplitude calibrator; output trigger, gate, sweep signals
-tolerates ± 10% line voltage variations

calibration service; local representative

1A1 dual-trace plug-in (ser. 014214)

-50 mv./cm. -20 V/cm.; DC-50 MHz.; rise time 7 nsec., 15 pF. input
-5 mv./cm/; DC-28 MHz.; rise time 12.5 nsec., 47 pF. input

011-0049-00 50Ω termination

-freq.-compensated over wide range

162 waveform generator (ser. 007495)

-pulse, gate, or sawtooth of adjustable

duration and repetition
- -externally or manually triggered
- -pos. pulse: + 0-50 V; 10 μsec. to 0.05 sec.; rise time ~1 μsec.; repetition 0.1 Hz.-10 kHz.
- -neg. sawtooth: amplitude decreases uniformly from 150 V to 20 V; duration 100 μsec.-10 sec.; repetition 0.1 Hz.-10 kHz.
- -output ~ 1000Ω
- -trigger: any pulse, into ~1 MΩ, pulse 15 V, 5 msec. or less rise time

161 pulse generator(ser. 006421)

- -to supply calibrated rectangular output or pos. gating pulse; variable delay on sawtooth input
- \- + 50 V gate, not adjustable
- -output impedance 1 kΩ max.
- -trigger sensitivity 3 V p-p min.; max. repetition rate 50 kHz.

163 pulse generator (ser. 1123)

- -to supply rectangular pulses of adjustable duration and amplitude; triggered by pos. pulse or sawtooth; variable delay on sawtooth
- -0-25 V p-p pulse
- -pulse output impedance 500Ω; varies with amplitude setting; min. load 3.5 kΩ

C-12 oscilloscope camera

E. H. Sargent and Co.
4647 W. Foster Ave.
Chicago, Ill.

S-84805 constant temperature water bath; circ. pump and heaters with separate controller (excl. contact thermometer)

- -heaters: 400 W fixed booster; 300 W adjustable uncontrolled; 250 W adjustable, controlled by saturable reactor; all switchable
- -regulation ± 0.01 C. and uniformity ± 0.01 C. to 70 C.; ±0.005 C. in vicinity of 25 C.

S-84810 water bath; Pyrex 16" dia. by 10" high

S-81840 mercurial thermoregulator (contact thermometer)

ASTM Ostwald-Cannon-Fenske viscometer

-inherent accuracy discussed for general type in NBS Monograph no. 55

The Gaertner Scientific Corp.
1201 Wrightwood Ave.
Chicago 14, Ill.

M342 micrometer slide (ser. 2352P)

-accurately ground and corrected lead screw and lap-fitted nut
-threaded carriage for mounting
-100 mm. (certificate 100.000 @ 20 C.), reading to 0.001 mm. with 10 part vernier; lead screw pitch 1 mm.

P. M. Tamson
Zoeltermeer, Holland

local: Neslab Instruments, Inc.
P. O. Box Y
Durham, N. H. 03824

TV40 viscometer bath (ser. 660239)

-0-230 C., ± 0.005 C. (0-100 C.)
-40 liters capacity, most inside controlled volume (baffled)

T3 circulation thermostat (ser. 0003635)

- ± 0.06 C. to 250 C.
-capacity 3.5 liters
-pump head 10', 130 gal./hr.

PBC-5 portable bath cooler (ser. 75043J)

-temperature control allowed to -15 C.

Englehard Industries, Inc.
Amersil Quartz Division
685 Ramsey Ave.
Hillside 5, N. J.

delay rods

-Amersil Optical Quality #2 , fabricated from specs on drawing 60037 (earlier 50012-1)

Keim Precision Mirrors Corp.
124 E. Angeleno Ave.
Burbank, Calif. 91502

silvering of delay rod ends (C.I.T. P. O. 25L-50364)

-on one face and 1" down adjacent sides
-10 max. resistance between any two points

Leeds and Northrup Co.
4901 Stenton Ave.
Philadelphia 44, Penn.

7556-1 guarded six-dial potentiometer (K-6) (ser. 1631257)

-high range 0-1.6 V in steps of 1.0 μv, ± (0.0005% + 1 μv)
-plus accessory standard resistors, adjustable DC resistors
-used for temperature measurements in conjunction with Pt thermometer below; cf. note by H. Strumpf to C. J. Pings on use of potentiometer for temperature measurements.

Platinum resistance thermometer (ser. 676711)

-calibrated by NBS, Nov. 18, 1949; certificate on file in Ch. E.; test no. 122106
-polynomial coefficients of resistance in temperature are in bounds

There is no record in any reports or notebooks by previous investigators, of the sources for the X-cut quartz transducers, or of the glass tubing blown into pycnometers, except for the cryptic notation about the transducers, "ex I.C.I." Transducers which are at least similar in performance can probably be obtained from Valpey-Fisher Corp., 1015 First Street, Holliston, Mass. 01746.

Other useful equipment, noted only by manufacturer or supplier:

Coaxial cables, BNC connectors: Belden; widely available
Submersible circ. pump: Little Giant Corp., Okla. City; distributed by Fisher Scientific
Syringes and needles: Becton, Dickinson and Co. "Yale" series with Leur-Lok needles; available readily through Bio. Dept.
Silicone grease: Halocarbon Products Corp., Hackensack, N. J.; does not tarnish platings

Remaining equipment: either standard items from stock or common fixed equipment, or fabricated from same according to mechanical drawings as noted in preceding text.

REFERENCES

1. J. H. Andreae, R. Bass, E. L. Heasell, and J. Lamb, Acustica 8,131(1958).

2. A. V. Anantaraman, A. B. Walters, P. D. Edmonds, and C. J. Pings, J. Chem. Phys. 44,2651(1966).

3. V. F. Nozdrev, Applications of Ultrasonics in Molecular Physics (Gordon and Breach, N. Y., 1963).

4. J. M. M. Pinkerton, Proc. Phys. Soc. B62,286(1949).

5. J. H. Andreae, P. D. Edmonds, and J. F. McKellar, Acustica 15,74(1965).

6. W. P. Mason, ed., Physical Acoustics (Academic, N. Y., 1964), Vol IA: a) 488; b) 364-5.

Appendix II. Operating Procedure

Our experiments lie in three groupings. First, a set of mixtures spanning the full range of mole fractions were carefully prepared and their densities measured on several isotherms. The data were used to compute excess volumes of mixing but more importantly to construct $\rho \longleftrightarrow \underline{X}$ calibration curves for pinpointing by density the compositions of samples made volumetrically for ultrasonics or viscosity measurements. The original data reported in notebook 5072: 43-61 and the more carefully taken later data recorded in notebook 5096: 11-13 are reduced to final density values in 5096: 11-13 and to excess volumes in 5096:56. Table I presents the results from the accurate later data. Second, a similar series of mixtures were prepared and the shear viscosities measured on three or four isotherms. The raw data are recorded in 5072: 43-61; 113 ff. and transcribed in 5096: 48-9. Values of η_s are computed at 5096: 54-5 and these in turn are fitted for temperature dependence to theoretical forms in 5096: 75-80. These results, which were used to construct figure 5 of paper II, are tabulated in Table II. Third, a similar series of compositions were prepared for ultrasonic absorption and velocity measurements. Actually, all the experiments were run several times with various improvements in the ultrasonic cell and procedure, before a satisfactory full set of data was obtained. Each mixture was prepared volumetrically, identified by density, entered into the sample cell, measured for α and β at four isotherms (when possible) accessed successively at four frequencies (4.5,7.5,10.5, and 13.5 MHz.) each time, rechecked for composition by density, and stored. Succeeding mixtures were prepared by enriching or diluting the previous mixture with lutidine. About every three compositions, fresh lutidine and distilled water were used, usually drawing from the same lutidine distillation batch as the previous set. The raw data require some discussion, particularly about diffraction and mode conversion corrections and error bounds, so we defer this presentation to Appendix IV. All equipment, chemicals, and procedures were thoroughly tested and calibrated as reported in Appendix III following.

Our specific procedure for accumulating the $\rho \leftrightarrow \underline{X}$ density calibration data is straightforward. The Tamson bath is warmed up while the pycnometers, weighing flask, and syringes are cleaned. The Tamson is trimmed to the first isotherm and the sample is made up by weight: the flask is weighed empty; one syringes out the approximate volume of lutidine into the narrow-neck weighing flask, then trims the weight drop-by-drop (quickly, to avoid evaporation and water pickup errors). The flask is stoppered and weighed. The procedure is repeated with the water portion, using a new or cleaned syringe. A sample is entered into the pycnometer with a small syringe and fine needle, with care to avoid forming bubbles in the pycnometer bulb or neck or to remove those that form. The pycnometer is equilibrated until 10 minutes after the liquid level stops visibly rising in the neck. After tapping loose any new bubbles, the volume is read and the Tamson reset for the next isotherm. After all four isotherms have been taken, the pycnometer is removed, its exterior and cap are dried with reagent acetone, and it is weighed, and finally cleaned.

The viscosity technique is similar. The Tamson is warmed up and the viscometer and syringes cleaned. The sample is made up approximately by volume in a 50 cc. flask and identified by density in a pycnometer much as above, at a reference temperature of 33.32 C. Two lengths of plastic tubing (one with suction bulb) are attached to the viscometer, which is then inserted in the bath and aligned vertically by a plumb line. One syringes as close as possible to 10 cc. of the sample into the viscometer, corks the tubing ends, and equilibrates the setup at the first isotherm for 15 minutes. The corks are removed and the suction bulb used to lift the sample to the proper level in the capillary arm. The time of flow between the fiduciary lines (around the upper bulb in our work, while this is not recommended in the NBS Monograph no. 55) is recorded. The timing is repeated twice more and then a new isotherm selected. Again, 15 minutes equilibration time is allowed before running. The composition was sometimes rechecked by density after the viscosity runs. The viscometer is then removed and cleaned with acetone.

Ultrasonic measurements are somewhat more involved, partly because of the complication of cell assembly. The Tamson and Sargent baths are warmed up. The alignment of the upper with the lower delay rod is checked by running them both into a close-tolerance Lucite tube made by the shop. Occasionally, we measured the additive constant for converting micrometer readings to absolute delay rod spacings. These must be known for diffraction corrections to the measured absorptions. Next the upper rod is removed and the cell proper is cleaned with acetone and seated on the lower rod. The upper plate and its stirrer are cleaned and fastened to the cell, with a strip of Teflon tape run around the cell lip for extra sealing. The stirrer drive is assembled. Circulation to the jacket is begun and one then checks for leaks to the inner cell. The Lucite box is assembled and its temperature control warmed up. Then about 350 ml. of sample is made up volumetrically. An aliquot is put into a pycnometer for identification by density. If the composition is too far from the desired one, the bulk sample is readjusted and rechecked by density. As the electronics are switched on to warm up, the sample is quickly poured into the cell through the delay rod hole. The Teflon collar is slipped onto the upper rod and the rod is put into the upper plate hole. The rod is clamped into the micrometer arm again and then the collar is tightened to the threading on the upper plate. For later runs, we also taped a Saran bag as a vapor trap to the collar on one end and to the upper part of the delay rod on the other. The Lucite box is closed, stirring is started, and the bath temperature is trimmed.

While the sample equilibrates, the electronics are tuned for the best received signal at the initial frequency (notebook 5072:80 records best tuning parameters). This entails switching to the optimum settings on the Chesapeake tuning dial, impedance matching box input and output taps, and Arenberg preamp input and output tuning slugs. The variable resistance on the impedance box and the resistances in and out on the Arenberg are adjusted by trial and error. Occasionally the Arenberg input capacitance or its tuning slugs may need attention, again by trial and error. One tries for maximum signal with a monotonic, smooth envelope. Sometimes the grease acoustical contact in one or the other transducer assembly gives out in part or in full, as evidenced by severe or total loss of received signal. Some pitfalls in the tuning procedure are noted in notebooks 5072: 127; 5090: 41 ff.

One is ready to start when the sample has equilibrated at least ½ hour with occasional stirring and the electronics are tuned. The predominant pulse frequency is measured by zero-beating the channel A-B added signals on the CRO. The average of the bath temperature in its cycling is recorded. The velocity may be measured first, as described in Appendix I. Care is taken to keep the micrometer and also the scope delay dial moving in one direction only, for any one set of height-delay measurements. This eliminates backlash errors in the delay dial, micrometer, and the riding of the Teflon collar upon the delay rod. After the β measurements, the α data are taken, again keeping the micrometer moving in one direction on any one pass. Generally we made three passes, up-down-up, to get three independent sets of data for better statistics. The first run is alway made <u>up</u>, to assure that the received signal is as large as possible on the CRO screen without going off the edges. The U-100 amplitude is adjusted to make the display fit. Of course, for all α and β measurements the stirrer is off. One must be careful that the signal is stable for the α data; if it visibly alters in size over periods of about 30 sec. it may give invalid data. Causes of instability include poor thermal homogeneity in the sample, especially at high lutidine concentrations where convection is easiest to set up; and poor 'sync' adjustment of the U-100. For some overall tuning, there may also be enhanced mode conversion errors, a form of overlapping and interfering echo in the delay rods that causes oscillations to be superposed on the monotonic decrease of amplitude with micrometer height. Since the oscillations are hard to characterize, they ruin the adaptability of the data to a linear least-squares fit. Any data run with gross disparities in micrometer intervals for succeeding db attenuation steps should be rejected and the apparatus should be retuned.

The tuning is all redone to reach the next frequency for α and β measurements, with only a nominal wait for restabilization of the electronics and with brief stirring of the sample, say 15 sec. After all four frequencies have been run, one changes the bath temperature and re-equilibrates the sample with occasional stirring for another $\frac{1}{2}$ hour. One finally runs through all four isotherms--or less, if one or two of the upper isotherms is in the two-phase region at the particular composition. By this time the sample has been in the cell about 8 hours. An aliquot is taken for rechecking the composition by density, and any visual turbidity is noted, as this may signal contamination by cell corrosion or jacket-to-cell leakage. While the aliquot is thermostatting, the upper plate of the cell is removed to expose the full sample, which is rapidly transferred to a storage flask using large 50 cc. syringes without needles. Electronics, enclosure heater, and bath are all shut down. The cell is disassembled and washed with acetone and air-dried. Finally, with the pycnometer data recorded, the Tamson is shut down and the pycnometer is cleaned.

Table I. Density Calibrations and Excess Volumes of Mixing

X(lutidine)	T(C.)	ρ, g./ml.*	est. ρ_{32}** V^e, ml./mole	est. $-(\frac{\Delta\rho}{\Delta T})_{32}$ #
0.9994	31.98	0.91144	0.91142	0.00089
	33.99	0.90966	0.000	
0.0000	32.00	0.99505	0.99505	0.00032
	34.00	0.99440	0.000	
0.0300	31.96	0.99228	0.99226	0.00046
	33.98	0.99135	-0.238	
0.0600	31.98	0.98978	0.98977	0.00064
	33.44	0.98883	-0.468	
0.0663	31.98	0.98921	0.98920	0.00067
	33.24	0.98837	-0.513	
	31.97	0.98924		
0.0901	31.98	0.98729	0.98727	0.00075
	33.46	0.98618	-0.684	
0.1240	31.98	0.98496	0.98494	0.00082
	33.50	0.98372	-0.926	
0.1769	31.98	0.98113	0.98111	0.00088
	33.50	0.97980	-1.267	
0.2100	31.97	0.97853	0.97850	0.00092
	34.02	0.97664	-1.452	
0.2996	31.96	0.97113	0.97109	0.00095
	34.04	0.96916	-1.853	
0.4003	31.96	0.96215	0.96211	0.00101
	34.04	0.96014	-2.110	

* ml. = 1.000027 cc.

** linear interpolation

linear interpolation, units g. ml.$^{-1}$ C.$^{-1}$

Table II. Shear Viscosities

X(lutidine)	T(C.)	ρ (g./ml.)	ν^{*} (centistoke)	η_s (centipoise)
0.0000	24.83	0.99711	0.8963	0.8937
	32.55	0.99487	0.7598	0.7560
	34.56	0.99421	0.7299	0.7257
	39.92	0.99227	0.6591	0.6540
0.0263 **	32.52	0.99239	1.234	1.225
	33.33	0.99202	1.214	1.204
	33.73	0.99184	1.203	1.193
	34.54	0.99149	1.183	1.173
0.0545	32.40	0.98998	1.895	1.876
	33.21	0.98949	1.914	1.894
	33.60	0.98926	1.980	1.959
0.0630	32.42	0.98922	2.058	2.036
	33.21	0.98870	2.085	2.061
	33.61	0.98844	2.151	2.126
0.0710	32.40	0.98855	2.194	2.169
	33.21	0.98800	2.211	2.184
	33.61	0.98773	2.276	2.248
0.0840	32.41	0.98742	2.386	2.356
	33.22	0.98684	2.369	2.338
	33.61	0.98655	2.371	2.339
0.1032	32.40	0.98599	2.580	2.544
	33.21	0.98538	2.531	2.494
	33.61	0.98507	2.507	2.470
	34.41	0.98446	2.474	2.436
0.1265	32.40	0.98442	2.785	2.742
	33.21	0.98377	2.717	2.673
	33.60	0.98345	2.686	2.642
	34.40	0.98279	2.624	2.579
0.1544	32.40	0.98245	3.025	2.972
	33.21	0.98177	2.943	2.889
	33.61	0.98143	2.896	2.842
	34.41	0.98075	2.820	2.766

(continued on next page)

---

* kinematic viscosity, $\nu = \eta_s/\rho$

Table II. Shear Viscosities (continued)

X(lutidine)	T(C.)	ϱ (g./ml.)	ν^*(centistoke)	η_s (centipoise)
0.177**	32.54	0.98063	3.126	3.066
	33.34	0.97993	3.039	2.978
	33.74	0.97958	3.000	2.934
	34.54	0.97887	2.914	2.852
0.2979**	32.54	0.97071	3.340	3.242
	33.34	0.96994	3.243	3.146
	33.74	0.96956	3.173	3.076
	34.54	0.96880	3.089	2.993
0.4017**	32.54	0.96145	2.840	2.730
	33.34	0.96065	2.766	2.657
	33.74	0.96025	2.732	2.623
	34.54	0.95946	2.663	2.555
0.9901**	32.57	0.91168	0.787	0.717
	33.36	0.91097	0.780	0.711
	33.72	0.91065	0.777	0.708
	34.53	0.90992	0.768	0.699

* kinematic viscosity, $\nu = \eta_s/\varrho$

** less reliable: poorer viscometer charge volume control and mole fraction determination

……………………………………

Shear Viscosity and Its Temperature Dependence at One Reference Temperature (33.2 C.) From Fit to Eq. (15) of Paper II

X(lutidine)	$\eta_{33.2}$	$(d \ln \eta_s / dT)_{33.2}$
0.0000	0.7460	-0.0204
0.0263 *	1.207	-0.0217
0.0545 *	1.894	+0.0167
0.0630 *	2.060	+0.0265
0.0710 *	2.184	+0.0108
0.0840 *	2.338	-0.0074
0.1032 *	2.494	-0.0236

(continued on next page)

---

* used second term in Eq. (15)

Table II. Shear Viscosity...Temperature Dependence...
(continued)

X(lutidine)	$\eta_{33.2}$	$(d \ln \eta_s / dT)_{33.2}$
0.1265 *	2.674	-0.0309
0.1544	2.888	-0.0359
0.177 **		
0.2979 **	3.156	-0.0406
0.4017 **	2.670	-0.0331
0.9901 **	0.712	-0.0129

* used second term in Eq. (15)

** less reliable basic η_s data; see table above

Appendix III. Calibrations and Tests

The first important calibration is that of the pycnometer volume, which was done with distilled water at four temperatures. The experiments are recorded in notebook 5072: 27 ff., while the data are reworked in 5096:4ff. The calibration was found to be better if no temperature coefficient of the volume was included. We note here that no buoyancy corrections were applied in the weighings with stainless steel weights. Since all the solutions are in a restricted range of density and the lutidine purity is no better than 99.5%, it does not appear worthwhile to rework the weight data. Some relative calibrations of the weights used (unrecorded) indicated that the uncorrected nominal masses give an accuracy of about 0.5 mg., within the error bounds of evaporation and water pickup in making the original $\rho \leftrightarrow \underline{X}$ identifications.

Lutidine purity is hard to determine quantitatively. Water content was assayed by Karl Fischer reagent several times (notebook 5072: 37 ff.; 5090: 152). It was held to 0.3 mole % for the initial $\rho \leftrightarrow \underline{X}$ identifications and to 0.06 mole % for final ultrasonic measurements. Freedom from isomers and homologs was not gauged; this requires gas chromatography. Only the claim of 99+% mole purity by the supplier (supported by a reported m.p., -7 to -4 C.) can be reiterated. The distillation after drying in our laboratory served more to draw the lutidine off the bed of drying agent than to remove homologs, which is better done by fractional crystallization, zone refining, or gas chromatography. The effectiveness of the new cell plating and sealing against contamination by cell corrosion (problems encountered: notebook *5072*: 50, 98, 102 ff., 127; *5090*: 114, 130 ff.) or evaporation can be weighed by the agreement of initial and final aliquot compositions in runs; also by lack of noticeable turbidity after sample runs. A final important aspect of mixture behavior over and above component purity is the establishment of our *practical* critical point $\underline{X_c}$, $\underline{T_c}$, to accurately gauge our distance from the same in any run. Our first attempts at $\underline{X_c}$ and $\underline{T_c}$ are recorded in notebook *5072*: 29 ff.; a limited coexistence curve mapping is done in *5072*: 74-8 to check the phase diagram published by Cox and Herington. We finally established $\underline{T_c}$ quite well at the same time that we used a platinum thermometer to calibrate our glass thermometers, check the Tamson bath stability (notebook *5090*: 145 ff., esp. 148 ff.). Notebook *5096*: 1 ff. reports some comments on the phase diagram and a closer determination of $\underline{X_c}$. Our best critical parameters are $\underline{X_c} = 0.065 \pm 0.001$ lutidine and $\underline{T_c} = 33.57$ C.

The accuracy and precision of our temperature measurements vary. Most viscosity, density, and ultrasonic data were taken with only calibrated glass thermometers for monitoring. The temperatures for viscosity and density are most reliable, as the experiments were performed in the closely-controlled and homogeneous Tamson bath. Temperatures in the ultrasonic cell are regulated by a poorer bath (Sargent) and in addition there is a temperature drop in transport of the circulating water. This drop, amounting to the 0.01 C. noted earlier, was measured by a zero-corrected thermocouple in test recorded in notebook 5096: 18, and used to adjust sample cell temperature records.

The $\rho \leftarrow\rightarrow \underline{X}$ identifications are actually calibrations and have no external checks. The shear viscosity data are better off, as the viscometer was calibrated with distilled water and reagent acetone (notebook 5072: 42 and 5096: 49-53-rework) using literature values for absolute water and acetone viscosities reported in the Handbook of Chemistry and Physics, edition 44, and *Techniques of Organic Chemistry*, ed. Weissberger, *et al*., respectively. The error bounds on the series of lutidine/ water mixture measurements, from differences in pressure head between calibration and run conditions, were noted according to N.B.S. Monograph no. 55 in notebook 5096: 49 ff.

In the ultrasonic experiments there are numerous possibilities for mechanical or electronic errors, either systematic or random. We recount below the numerous checks we performed, except for measurements of the principal systematic errors discussed with the data reduction schemes in Appendix IV. We might mention that these main correctible errors are in the delay dial calibration, for velocities, and in the attenuator calibration, diffraction correction, and mode conversion, for absorption. Also in the final data reduction, the visual CRO screen reading error and the remaining systematic and random errors discussed below are lumped into an equivalent random error source.

We first consider the mechanical aspects of sound propagation. Before acoustic mode conversion in the delay rods was identified as the major source of signal drift, we looked for mechanical errors in the micrometer alignment and travel. The micrometer precision was checked with a travel indicator over short ranges (notebook _5072_: 88). The effects of angular misalignment of the delay rods upon the amplitude and envelope of the received signal were checked with a goniometer replacing the micrometer (notebook _5090_: 60 ff.). The resultant signal variations with angle were recorded photographically. No clear leads resulted, but it became apparent that alignment was not as critical as thought previously for either absolute signal levels or for relative change with height. The simple procedure of aligning the two delay rods before the run by use of a Lucite tube is certainly adequate. The smoothness of finishes on the delay rod faces also does not seem critical, as the lower Duralumin face deteriorated visibly without bad effects. Binding of the Teflon collar against the moving upper rod _did_ cause signal variations, but this was carefully avoided during each run. (notebook 5072: 129; 5090: 77). A final mechanical cause of signal variation is a variable load on the transducer housings, hence on the transducer-rod contacts. In the misalignment tests, we sometimes loaded the housing with extra weight with its collet untightened and achieved significant fractional increases in the received signal. Conceivably the pull exerted on the top housing by the RF cable could cause a smaller but still bad effect. Keeping the collet tightened eliminated the error. General accounts of signal drift errors we encountered are given in notebooks 5072: 88-90, 104 ff.; 5090: 29, 32, 35, 39 ff.

Electronic contributions to error are minimized first by using the best tuning, i. e., the simplest monotonic envelope for the RF signal. Overtones, harmonic and FM distortion in poorly-shaped pulses cause spuriously high losses (see Nozdrev, ref. 3 of App. I) and accentuate the mode conversion problems. Instability of gain at the Arenberg preamp caused repeated problems, to the point of requiring some experimental runs to be abandoned. The linearity of the Arenberg and of the two CRO channels as a unit was verified after completing the ultrasonic experiments, by dividing a variable-amplitude signal between the two circuits (notebook 5096: 41-2, 46-8). Stability of the CRO in gain and sweep was unquestionably excellent. The comparison signal amplitude is also very stable. Initially there was a problem because its rectangular wave modulation had a slope, but this was eliminated (notebook 5090: 77) by bypassing an electronic module providing DC bias to the signal (part of the original design we inherited). The stability of the laboratory temperature probably aided that of all the electronics.

Frequency accuracy depends upon the comparison signal generator, the HP 606A. We frequently recalibrated its vernier dial against its internal beat frequency oscillator overtones. The BFO itself was checked against a Beckman counter (notebook 5096: 43-5) and found to be well within specifications. The visual beat technique for measuring received signal frequency by comparison to the reference signal worked much more simply and at least as well as the alternative, matching a whole series of peaks in the two signals displayed expanded upon the screen.

Several total calibration runs were made on benzene, with the apparatus in various stages of improvement. Benzene's α and β values are well known (ref. 7, paper II) and are taken as standards. Our apparatus and procedure seem to give good results by this check (notebook 5072: 91; 5096: 34). Our sound velocity measurements in water (notebook 5096: 35-7) indicate no dispersion with frequency, which again agrees with the literature.

Appendix IV. Ultrasonic Data Reduction and Results

We first consider the absorption data, composed of two to six sets of micrometer height (h): attenuation readings for each of 144 conditions of composition, temperature, and frequency (*X,T,f*). Reduction of the data to α values for each of the 144 conditions (denoted by some index *k*) is done in two basic steps. First, each full set of points, denoted by some double index *kn* and composed of N_{nk} individual points, is least-squares fit to the linear form $a_i^{kn} = \alpha_n^k h_i^{kn} + b_n^k$ (for $i=1,N_{kn}$ in FORTRAN-style notation). Second, the various values of α_n^k of absorption computed from each of the N_k data sets are combined into a weighted average α^k, taken as our best approximation to the true absorption in the state *k*. In other words, the α_n^k are fit to the constant form $\alpha_n^k = \alpha^k$.

In practice, the fitting procedures are quite complicated, for two reasons. First, we must correct the raw data points a_i^{kn}; h_i^{kn} for systematic errors. Second, we must assign them realistic error bounds so that we can finally estimate the error bounds of the α^k. The following elaborations are incorporated into the reduction scheme:

-*Firstly*, some data sets *kn* recorded in the notebooks have obvious systematic errors, the presence of which was noted at the time of the experiment. Signal instability from poor tuning, from convection currents in the cell, or from faulty preamp operation is the usual culprit. These data sets are not even used.

-<u>Secondly</u>, the raw attenuation readings a_i^{kn} are corrected for two systematic errors, before fitting. Errors in the micrometer readings h_i^{kn}, in the instrument or in observation are so low as to be negligible. The first systematic error is the deviation of attenuator readings on the HP 355C from actual attenuations. These actual attenuations were measured after the completion of experiments by sending the attenuator to Hewlett-Packard in Palo Alto. Calibrations at 4.5 MHz. and 13.5 MHz. are recorded in notebook <u>5096</u>: 80-81. and are incorporated in the computing to translate readings to true net attenuation.

Second and more important is the correction for diffraction losses in propagation of the pulse through the liquid. A finite-area transducer does not produce a collimated column of plane waves; rather, the beam spreads over some angle and attains a warped amplitude profile. The former causes incomplete exposure of the lower transducer to the total radiated energy. The latter causes destructive interference in signals generated across the lower transducer face, hence rejection of a portion of that power impinging on the trasnducer. The shape of the sound amplitude or velocity field equivalent for two finite circular transducers is governed by ordinary hydrodynamics. R. Bass (J. Acous. Soc. Am. <u>30</u>,602 (1959)) presents calculations on the theory. We had to extend these to shorter distances between transducers, with a new expansion of the integrand in the integral representation of the loss factor. We also verified the additivity of diffraction losses to true absorption, intuitively and numerically. Details of all our calculations will be presented later in this Appendix.

The apparent diffraction loss Q depends upon the absolute delay rod spacing z, obtained from the micrometer reading through an additive constant h_o. This constant was occasionally measured for the assembled apparatus. Thus we represent the total measured attenuation (translated from the nominal attenuation setting) α_i^{kn} as

$$\begin{aligned}\alpha_i^{kn} &= A_i^{kn} + Q(z)\\ &= A_i^{kn} + Q(h_i^{kn} + h_o),\end{aligned}$$

where A is the true sample absorption plus any random errors. The actual least-squares fit is then

$$A_i^{kn} = {}_n^k \, h_i^{kn} + b_n^k \, .$$

-Thirdly, we assign estimated errors to each data point α_i^{kn}. First is a constant error σ_1 from random fractional changes in signal amplitude, in turn due to generator fluctuations or to sound-refracting convection in the cell. σ_1 is given in our original notebook work and in our computing in terms of equivalent fluctuations in CRO display height at a nominal total height of I_o (=7 cm. usually). We take σ_1 to be 0.06 cm. for our runs, which converts to 0.074 db. Second is a scope-reading error σ_2 in matching comparison and received signals, roughly 0.15 mm. for us. Mismatch of the traces by a height σ_2 at a nominal display height of $I = I_0 e^{-a/8.686}$, where a is attenuation as usual, gives an error in attenuation δa,

$$\begin{aligned}\delta a &= \left(\frac{\partial a}{\partial I}\right)\delta I \\ &= \left(\frac{1}{8.686\ I}\right)\sigma_2 \\ &= \frac{\sigma_2}{8.686\ I_0}\, e^{a/8.686}.\end{aligned}$$

The net estimate error is

$$\sigma_i^{kn} = \frac{1}{8.686\ I_0}\left[(\sigma_1)^2 + (\sigma_2\, e^{a_i^{kn}/8.686})^2\right]^{\frac{1}{2}}.$$

This error estimate is used first to weight the data points relative to one another, for we perform the least-squares fit by minimizing the error function

$$\chi^2_{kn} = \sum_i \left(\frac{A_i^{kn} - \alpha_n^k h_i^{kn} - b_n^k}{\sigma_i^{kn}}\right)^2.$$

Clearly, data points at high attenuations are weighted less, as they are more error-prone. For the averaging fit of the α_n^k to α^k, the estimated error σ^{α}_{kn} in each α_n^k is compounded from the presumably independent pointwise errors σ_i^{kn},

$$(\sigma^{\alpha}_{kn})^2 = \sum_i \left(\frac{\partial \alpha_n^k}{\partial A_i^{kn}}\right)^2 (\sigma_i^{kn})^2.$$

Similarly, α^k, our best approximation to the true sample absorption, is a weighted average,

$$\alpha^k = \sum_n \frac{\alpha_n^k}{(\sigma_{kn}^\alpha)^2} \Big/ \sum \frac{1}{(\sigma_{kn}^\alpha)^2} ,$$

from minimizing

$$\chi_k^2 = \sum_n \left(\frac{\alpha_n^k - \alpha^k}{\sigma_{kn}^\alpha} \right)^2 .$$

Its error compounds as

$$\begin{aligned} (\sigma_k^\alpha)^2 &= \sum_n \left(\frac{\partial \alpha^k}{\partial \alpha_n^k} \right)^2 (\sigma_{kn}^\alpha)^2 \\ &= \frac{1}{\sum_n (\sigma_{kn}^\alpha)^2} . \end{aligned}$$

All the fits and error computations are done in a comprehensive computer program, which is flowcharted later. σ_k^α is not necessarily the final estimated error, and it is not the only information we have on error levels--we also have χ^2_k. The rescaling of errors and final confidence levels in the α^k are discussed under the sixth heading here.

-Fourthly, in both the N_k individual linear fits for the α_n^k and the final averaging for α^k, we exercise the option of deleting data points on either of two grounds. The first ground is automatic: a 3-σ test is run on each data point i in turn. This means that Q_i^{kn} and h_i^{kn} are tentatively deleted and a new fit made to the remaining N_{kn}-1 points. If the point i ends up more than 3 standard dev-

-iations $3\,\sigma_n^k(i)$ from the line of tentative fit, it is permanently deleted:

$$\text{Compute } R = \left| \frac{A_i^{kn} - \alpha_n^k(i)\, h_i^{kn} - b_n^k(i)}{\sigma_i^{kn}} \right| ;$$

$$\text{If } \begin{cases} R \geq 3, & \text{delete the point} \\ R < 3, & \text{retain it.} \end{cases}$$

More than one point may be a candidate for deletion, but the program took only the latest one; we redid several choices by hand, taking the one giving the lowest χ_k^2 (the notebook 5096 is corrected as of 7/13/71). Overriding the program choice in the case of nearly equivalent deletions calls for discretion, and is discussed in section 6, with details. If there were fewer than 4 data points to begin with, $\underline{N_{kn}} < 4$, the 3-d test could not be run.

The second ground for rejection is the discretion of the user. Optional input to the computer program forces a deletion of the point $\underline{i}$ and displays the resulting α_n^k or α^k. In the former case, it does not alter the automatic inclusion of α_n^k from the automatically-selected 'best' deletion in the final averaging for α^k. If the deletion, on the basis of some observation during the experiment (recorded in the notebook), looks like a more reasonable and reliable course, the final α^k must be manually recomputed. We exercised this option several times, but did not choose to alter the automatic results. We also tried some forced deletions in the final averaging of the α_n^k and did excise a number of runs.

-*Fifthly*, we tested for the presence of other systematic errors. The most likely error is a constant mismatch of the CRO displays in *one* direction (so it is not random). Since the received signal has a fluttering noise band at the outer edge of its envelope, we might by accident take the outer fringe of the total (noise + received signal) envelope to match the edge of the comparison envelope. Another possible error is insufficiency of the diffraction corrections. Either error changes the form of the equation our data should fit; our first guess was a quadratic,

$$A_i^{kn} = \gamma_n^k \, (h_i^{kn})^2 + \alpha_n^k \, h_i^{kn} + b_n^k.$$

Now, the reduction of the data to net error functions χ^2_{kn} is *not* an adequate indication of the systematic error. That is, a quadratic fit yielding a lower χ^2 than a linear fit is not necessarily preferred. F. Sculli of physics clarified this in several discussions we had (notebook *5090*: 123-4; *5096*: 76); least-squares fits are simply not good indicators of systematic error, except in the following sense. If the quadratic coefficient γ_n^k improves χ^2 and *also* ends up with an attached error σ^{γ}_{kn} sensibly smaller than itself, say $\sigma^{\gamma}_{kn} < \frac{1}{2}\gamma_n^k$, then it is probably warranted in the data representation. Conversely, inclusion of a γ_n^k which has an error $\sigma^{\gamma}_{kn} \gtrsim \gamma_n^k$ is unwarranted regardless of its effect on χ^2 and does not represent the systematic error.

The quadratic terms in our typical tests were small, but they drastically altered α_n^k and increased σ^{α}_{kn} (notebook 5096: 63). We analyzed the form of the matching error more carefully. Consider a received signal at zero attenuation with envelope height I_1 composed of the true received signal envelope I_1^o plus a constant noise band c. It is matched to the comparison signal I_0, at a micrometer reading h_0:

$$I_1 + c = I_0.$$

Now, at an apparent attenuation of n db, the received signal is actaally attenuated by n_0 db:

$$\begin{aligned} I_0' &= I_0 e^{-n/8.686} \\ &= (I_1') + c \\ &= I_1^o e^{-n_0/8.686} + c. \end{aligned}$$

Here n_0 is presumably linear with acoustical path,

$$n_0 = \alpha(h_n - h_0).$$

Rearranging, we find the relation of n_0 and n to be, for small c,

$$n_0 \simeq n + 8.686(\frac{c}{I_0})(e^{n/8.686} - 1) = \alpha(h_n - h_0),$$

and so a better equation for least-squares fitting the A_i^{kn} is

$$A_i + \underbrace{8.686\gamma(e^{A_i/8.686} - 1)}_{} = \alpha h_i + b.$$

Trials of this equation showed a strong coupling of γ and α (large changes in α and large values of σ^{γ} and σ^{α}), which were recognized as coming from the A_i-like term in the underbracketed term above. This was deleted to give

$$A_i + \gamma\left[8.686(e^{A_i/8.686}-1) - A_i\right] = \alpha h_i + b.$$

Now α was not drastically altered from its linear fit value. Significantly, in all conditions *k*, γ was small and $\sigma^{\gamma} \gg \gamma$, so we concluded there is no significant systematic error we had not corrected.

-*Sixthly*: Eventually, we had all our results $\{\alpha^k_n;\ \sigma^{\alpha}_{kn};\ \chi^2_{kn}\}$ and $\{\alpha^k;\ \sigma^{\alpha}_k;\ \chi^2_k\}$. These are partly reproduced in Table II. In four runs *kn* we chose to reject the point deletion giving the lowest χ^2_{kn}. In three cases (*k*=[*X*=0.2132, *T*=34.66, *f*=4.5], *n*=5; *k* =[0.0436,33.84,4.5],*n*=4; and *k* = [0.0664,32.66,4.5],*n* =1) there were two deletions giving very similar χ^2_{kn} and σ^{α}_{kn} but very different α^k_n (points 4&1, 5&1, 6&1, respectively), so we averaged them. In the fourth case (*k* =[0.0288,34.64,7.5],*n* =3), deleting point 5 gave a slightly better χ^2_{kn} than did deleting point 4, but also a much larger σ^{α}_{kn}, so we chose the latter.

No entire run *kn* was rejected automatically by the 3-d test in averaging. We rejected some runs in each of 3 conditions *k* on extrinsic grounds. For *k* =(0.0722,32.66, 7.5) we eliminated runs 1-3, which were noted during experiments as having unusual signal tuning. They also gave very much different α^k_n than the last 3 runs. For the two states *k* =(0.0664,32.66,7.5 and 10.5) we took only the good-tuning reruns, and in the first of these we also rejected the first rerun, noted as having less reliable tuning.

The complete set of reduced data can be examined in a computer output binder on file, containing the original output in a fully explanatory format. Deletions on discretion noted above, as well as manual selections of the best deletions over the original program's automatic choice of latest deletion, are noted in a separate standard portfolio, which also contains the raw data, program listings, condensed output (from punched cards), and table of deletions for all states.

The results are to be interpreted as follows. The *relative* error estimates for the data points A_i^{kn} or for whole runs α_n^k are probably accurate, for weightings in their respective fits. The absolute error levels, however, may not be. If we desired our error estimates σ_1, σ_2 to represent bounds on the true error with a confidence level of *C* (say, 50%), then the *grand average* of $\chi^2_{kn}/(\underline{N_{kn}-F}) = \chi^2_{kn}/(\underline{N_{kn}}-2)$, $\bar{\chi}^2$ (*F* =degrees of freedom in fit) should reflect this value of *C*. Thus $\bar{\chi}^2$ should be 1 for *C* =50%; 1/9 for *C* =95%; etc.). The specific relation is

$$C = \int_{\bar{\chi}^2}^{\infty} e^{-P^2}\,dP.$$

$\bar{\chi}^2$ should be adjusted to the proper level by uniformly rescaling all the errors σ_1, σ_2:

$$\left.\begin{array}{l}\sigma_1\rightarrow P\sigma_1\\ \sigma_2\rightarrow P\sigma_2\end{array}\right\}\Longrightarrow\ \sigma_{kn}\rightarrow P\sigma_{kn}\ \Longrightarrow\left\{\begin{array}{l}\chi^2_{kn}\rightarrow P^{-2}\chi^2_{kn}\\ \chi^2_{k}\rightarrow P^{-2}\chi^2_{k}\\ \bar{\chi}^2\rightarrow P^{-2}\bar{\chi}^2\end{array}\right.$$

Choose $\underline{P}$ to give proper $\bar{\chi}^2$.

This is a legitimate adjustment in the least-squares technique, as much as we can do without taking additional measurements to establish that σ_1 and σ_2 should scale differently. New error estimates change the results of the 3-d tests of course, and the whole data set should be rerun. If the new 3-d tests do not significantly alter the choice of data deletions, then the iterated $\bar{\chi}^2$ should still be near its desired value. We note that the σ's should represent 50% intervals for the 3-d test as given on p. 190; the break factor $\underline{B}$ should be adjusted for any other confidence level.

In practice, we decided that the $\underline{N_k}$ groups of data seta for the $\underline{k}$ conditions are more on an equal footing of reliability than the $\underline{N_{kn}}$ individual data sets. Thus we computed $\bar{\chi}^2$ and the tentative rescale parameter $\underline{P}$ as

$$P = (\bar{\chi}^2_{old})^{-\frac{1}{2}} = \left(\frac{1}{N}\sum_k\left[\frac{\sum_n \chi^2_{kn}}{N_k}\right]\right)^{-\frac{1}{2}}.$$

Our initial estimates of the σ's were too conservative, as our first $\underline{P}$ value was 0.30. We redid all the fits and got a more acceptable $\bar{\chi}^2$. Interestimgly, the new $\underline{P}$ broken down by frequency $\underline{f_k}$ showed a systematic trend,

f, MHz.	P	f, MHz.	P
4.5	0.48	13.5	0.72
7.5	0.76		
10.5	0.52		

This probably indicates that σ_1, σ_2 are not the same for all f due to differences in envelope shape, generator stability, etc. We did a 'final' rescaling, different for each f, using the computed P(f) on the previous page. We readjusted σ_k^α and χ_k^2, but did not redo the fits.

Finally, we did a further averaging of the new σ_k^α over the three isotherms T for any given X and f, since ${}_k$ and σ_k^α varied little with T. We obtain better statistics on σ_k^α. Unfortunately, one flaw remained in our data: the average $\chi_k^2/(N_k-1)$, $\bar{\chi}_k^2$, which measures the scatter of the results α_n^k about α^k, was too large. While the data points in individual runs scattered little--the correct amount after rescaling, the results α_n^k scatter more than the errors σ_{kn} from data point scatter would indicate. Since the final errors σ_k^α are the most importnat, we rescaled errors once more, doubling all σ's. Then the average over k of $\bar{\chi}_k^2$ came to near unity.

In the final results in Table III, we quote α_{ex}/f^2, after subtracting classical shear losses α_{cl}/f^2 and a mode conversion correction discussed immediately below. The errors σ_k^α collapsed over the 2 or 3 isotherms, σ_{Xf}^α, indicate the bounds of the corresponding $\alpha^{XfT} = \alpha^k$. The associated confidence levels χ_{Xf}^2 are collapsed once more over f to a χ_X^2, which indicates the confidence one can have that the errors σ_{Xf}^α truly represent the error bounds. The χ_X^2 average to unity, of course, but the value for each X may scatter around this. The scatter may be real, and so we do report the individual X_X^2.

Our data looked good as far as error estimates were concerned. Still, it had indications of one last systematic error, this one in *frequency* and not in attenuation readings. At high mole fractions of lutidine, far from the compositions showing chemical or critical relaxation, mixtures should behave as Kneser liquids with high relaxation frequencies. The frequency dependence of α/f^2 should be nil. Also, any f-dependence of α/f^2 that does develop toward lower X should consist of a monotonic *decrease* with increasing f. However, the four most concentrated mixtures,

$\underline{X}$ = 0.9901, 0.427, 0.3823, and to some extent, $\underline{X}$ = 0.3042, the values of $\alpha/\underline{f}^2$ at 7.5 MHz. dip lower than those at higher $\underline{f}$. Also, the values at 4.5 MHz. are notably higher than the values at 10.5 and 13.5 MHz.; the rise at 4.5 MHz. is too rapid even for strong thermal relaxation at low frequency of unknown origin.

The possible errors in $\alpha/\underline{f}^2$ at $\underline{f}$ = 4.5 and 7.5 MHz. tie in with observations during the experiments that at these same frequencies the ultrasonic pulses showed unstable shape and extra oscillations in amplitude versus height. After some searching in the acoustics literature, we finally discovered a reference to a similar phenomenon in Puls' thesis (ref. 19, paper II), called <u>mode conversion</u>. The sound pulse is slowed and distorted at the walls as it travels down the delay rod, forming a longer, self-interfering wavetrain. The oscillatory displacement of the delay rod face, generating sound in the liquid sample, is then not plane; not of the same amplitude and phase across the face; i.e., not of a pure vibration mode. A recent journal article (H.J. McSkimin, J. Acous. Soc. Am. <u>31</u>,287(1959)) suggests breaking up the spurious modes by roughing the rod walls, as by cutting a screw thread in them (Puls). Since mode conversion (MC) causes spurious spreading and interference in the beamed sound pulse much as diffraction does, it is likely an additive attenuation. The net loss probably depends upon the total range of micrometer readings, so a simple uniform correction depending upon f but not the value of α is not justified. However, α/f^2 does not vary much with X at these high concentrations of lutidine, so we will apply a uniform correction of -30 ($\times 10^{-17}$ Np. cm.$^{-1}$ sec.^{2}) to α/f^2 at $f = 4.5$ MHz., and a similar one of +8 in these units at $f = 7.5$ MHz. Toward lesser X this is not accurate but α/f^2 grows so large that a small feature in error does not qualitatively change our data or its interpretation.

Our final α/f^2 data for the 144 conditions of X, T, and f are reported in Table III, after incorporation of the MC correction and after subtraction of the classical loss $(8\pi^2\eta_s)/(3\rho\beta^3)$ listed at the side. Water data are taken from the literature, since MC problems here swamped the measurements.

Velocity

The velocity data are composed of one set of micrometer height (h): signal delay (t) readings for each of the conditions k, except for a very few cases with two or three sets. One linear least-squares fit reduces each data set to a velocity ,

$$h_i^k = \beta^k t_i^k + c^k \text{ .}$$

The frills in the reduction scheme parallel those for α :

(1) Some poor data sets were rejected outright and the run remade immediately during the experiments.

(2) delay time readings, from the variable sweep delay dial of the CRO, are corrected to the true delay times

according to the calibration made with a Beckman counter, as noted in Appendix III. A quadratic fit of the true delay to the dial readings was used (notebook 5096: 81). This is a very minor correction.

(3) we assign errors to each delay reading, σ_i^k. The inherent reproducibility, high accuracy, and low data scatter we noticed suggests that our main dial error is the failure to read half-divisions, so we picked $\sigma_i^k = 0.005$ turns uniformly. Each turn represented a delay of 5 μsec. usually. We obtain a confidence level function χ_k^2 and an estimated error bound σ_k for each run.

(4) we had a feature to delete data points automatically or on discretion. The 3-d tests were used uniformly, selecting the one giving the best χ_k^2, by hand if necessary. One run had an obvious error in recording of one delay reading, which we corrected manually.

(5) quadratic fits were made to test for systematic errors, and again none were found.

(6) the error information σ_k and χ_k^2 were interpreted as for κ. Our initial fits indicated a rescale of error to an almost uniform 0.1%. We think 0.3% is a more reliable estimate for all states k. Only the 4.5 MHz. values are reliable, free of the systematic error from envelope-shape change discussed in Appendix III--except that the underlined β's at f = 7.5 or 10.5 MHz. were done by the tedious peak-watching technique and are also reliable. The

results are given, without the trivial σ_k or χ_k^2, in Table III.

Fit Program 'Flowchart' and General Organization

A FORTRAN program was written for the IBM system 360/370 to fully process the raw data for absorption and velocity. Input is divided into groups, one for each of the 144 conditions (X,T,f). Each group is composed of first the α data, then the β data. The first card in the group is an (X,T,f) identification and remark card. An optional card before this (recognized by its format) may update the estimates of the micrometer-to-acoustical path correction h_o and of the zero-db display height I_o. Another optional format-recognized card (OFRC) before the actual absorption data updates the error estimates σ_1, σ_2; and another before the velocity data updates o for that data. The entire program is too large to list in the thesis, just as is the raw data set; both are on file in a computer binder and in a standard portfolio. The FORTRAN-style outline follows, keyed to actual statement numbers.

(final version)

```
 2 read X,T,f,title
     if OFRC, read $h_o,I_o$
   reread X,T,f,title
   if $X=X_o$ go to 10
     store new $X_o$
     write compendium of results for old $X_o$
10 write title; new $h_o,I_o$ if changed

          [$\alpha$ section]

   read $N_k$
     if $N_k = 0$, go to 220 ($\beta$ section)
```

```
    do 100 $n = 1,N_k$
      read $N_{kn}$
        if OFRC, read $\sigma_1$, $\sigma_2$
      write title
      read  the $h_i^{kn}$ and echo them; convert to z
         values for diffraction correction; assume
         the $a_i^{kn}$ are in progression from 0 to $N_{kn}-1$
         unless another OFRC tells us it starts
         from $n_o$
      compute diffraction corrections $Q(h_i^{kn} + h_o)$ by
         interpolating data table cubically; first
         correct table to proper f
      write out $A_i^{kn}$ for inspection
      compute $\sigma^2$
    call for linear fit; routine called writes out
        all the relevant information $\alpha_n^k, \sigma_{kn}^{\alpha}$, and $\chi_{kn}^2$
        and returns all for later averaging; also
        returns flag to denote if, and which, data
        point was deleted
    (do optional discretionary deletions and refits)
     read $M_{kn}$ = no. of purges to be run on this one
        data set
     call linear fit, printing same as above (do
        not store results)
     call quadratic or other nonlinear fit
100  (call purged nonlinear fit)
     write out compendium of results for linear fits
        for conditions k, plus averaging of same
        esp. for rescale parameter
     call point-fit (average) of all the $\alpha_n^k$; routine
        called prints all results $\alpha^k$, $\sigma_k^{\alpha}$, and $\chi_k^2$
     (call purged point fits)
     write out compendium of results for nonlinear
        fits
     call average of all $\alpha_n^k$ for nonlinear fits
     (call purged fit of same)

              section

     read $N_k$ (0 or 1)
       if $N_k = 0$, go to 2 for next group of data
     read $N_{1k}$, $\sigma$; convert latter to $\sigma_i^k$ (same for all
        i)
     read the $h_i^k$, $t_i^k$ and echo them
     correct $t_i^k$ by parabolic fit
     call linear fit, printing $\beta^k$, $\chi_k^2$
     (formerly, call quadratic fit)
     go to 2
```

terminates by read error, end of data set